Anna Katharina Neumayer, BSc

Double RNA *trans*-splicing induced gene repair in *COL7A1*

MASTER'S THESIS

to achieve the university degree of

Master of Science

Master's degree programme: Molecular Microbiology

submitted to

Graz University of Technology

Supervisor

Ao. Univ.-Prof. Dipl.-Ing. Dr.techn. tit.Univ.-Prof. Günther Daum

Institute of Biochemistry

Dr. Ulrich Koller, Laboratory of epidermolysis bullosa research, EB-House Austria

Graz, October 2016

AFFIDAVIT

I declare that I have authored this thesis independently, that I have not used other than the declared sources/resources, and that I have explicitly indicated all ma-terial which has been quoted either literally or by content from the sources used. The text document uploaded to TUGRAZonline is identical to the present master‘s thesis.

Date	Signature

Acknowledgements

First of all I am particularly grateful to Univ.-Prof. Dr. Günther Daum not only for accepting this topic and supervising me.

I would like to thank Univ.-Prof. Dr. Johann Bauer for giving me this great opportunity to work in the EB-House Austria in Salzburg.

Furthermore I would like to especially thank Dr. Ulrich Koller and Clemens Hüttner, MSc for co-supervising me over this period of time in the lab, all the scientific input, help and support when difficulties arose and for proof-reading of my master thesis.

I am grateful to all my colleagues in the EB-House team, particularly to the members of the House C lab for the unforgettable time and all the laughing throughout my whole time in the lab. I would like to especially thank Bernadette Liemberger for her help and proof-reading of my master thesis.

My special thanks to my family and my friends for their support during my entire study. Especially I would like to thank my mum Beatrix Neumayer and my friend Melanie Kienzl for always being ready to lend an ear, for building me up and supporting me.

At last I would like to thank my boyfriend Anton Kaufmann for always being there for me and backing me up all the time.

This master thesis was funded by FWF Austrian Science Fund (P25304-B19) and DEBRA Austria.

Table of Contents

Abstract

The recessive dystrophic variant of the blistering skin disease epidermolysis bullosa (RDEB) is caused by mutations within the *COL7A1* gene encoding type VII collagen building up the anchoring fibrils within the basement membrane zone of the skin. RDEB causing nonsense mutations in *COL7A1* lead to the loss of type VII collagen resulting in instability of the skin and blister formation. The main aim of this study was the exploitation of the double RNA *trans*-splicing technology for the specific repair of a homozygous mutation within exon 105 of *COL7A1* at pre-mRNA level.

In recent years RNA *trans*-splicing evoked to a promising technology to repair gene mutations on RNA level. Thereby the endogenous splicing machinery is used to recombine a designed RNA *trans*-splicing molecule (RTM) with endogenous target pre-mRNA and the disease-associated target region is replaced by its wild-type version. Using a previously developed fluorescence-based screening system we have selected a highly efficient double RNA *trans*-splicing molecule (dRTM) for further repair studies in RDEB patient keratinocytes. The dRTM comprises the wild-type coding region of *COL7A1* spanning from exon 103 to exon 105, flanked by two splicing domains and two binding domains, targeting intron 102 and 105, respectively, for simultaneous induction of 3' and 5' RNA *trans*-splicing. Accurate double RNA *trans*-splicing leads to the specific exchange of exons 103-105, including the disease-associated mutation, with the wild-type *COL7A1* sequence provided by the dRTM. In order to increase the double RNA *trans*-splicing efficiency we further utilized the screening system to study the impact of antisense RNAs (asRNAs) on the *trans*-splicing characteristics of the selected dRTM. We showed the possibility to increase the *trans*-splicing efficiency via quantifying the readout for accurate *trans*-splicing between the dRTM and a designed *COL7A1*-minigene by the level of GFP expression. The most promising antisense RNA (asRNA 9), binding 340 bp of *COL7A1* (intron 104), was capable to increase the *trans*-splicing efficiency of the selected dRTM up to three-fold.

After viral transduction of the most efficient dRTM into patient keratinocytes the restoration of type VII collagen expression was detectable via immunofluorescence staining. Thus we assume that RNA *trans*-splicing is a promising strategy for the repair of mutations in *COL7A1*.

Especially our fluorescence-based screening system is a versatile tool to either accelerate or facilitate dRTM design and construction, or to study other factors influencing the *trans*-splicing behavior of a given RTM prior to experiments in type VII collagen deficient patient cells.

1 Introduction

1.1 The human skin – function and morphology

The human skin is with 3,5 to 10 kilos and 1,5 to 2 square meters size the largest organ of the human body. The skin protects the human body against environmental conditions like cold, heat and humidity; it serves as sensor and body thermostat to keep the body temperature. Water, metabolic substances, etc. can be stored in the skin. Furthermore, the skin is involved in vitamin D synthesis and wound healing [1]. The normal human skin is composed of three major layers: directly exposed to the environment is the epidermis, followed by the dermis, which is separated from the epidermis by the dermal-epidermal junction and finally the hypodermis at the bottom [2]. The skin contains blood vessels, hair follicles, nerves, lymphoid vessels, etc. (Figure 1).

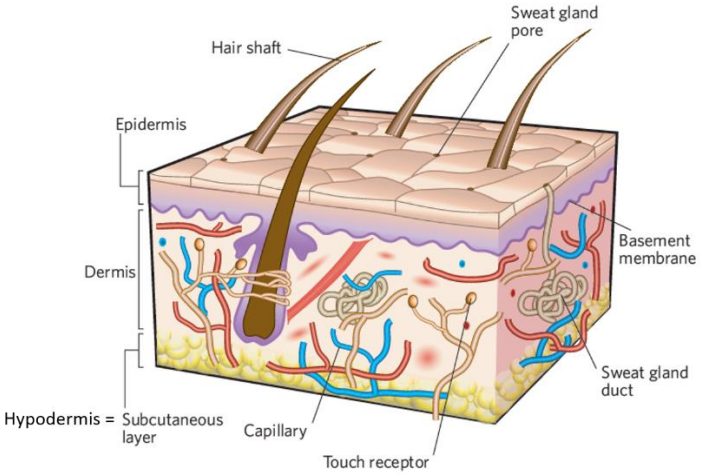

Figure 1. Depiction of the skin showing the different major layers. All contained cells and important structures, like blood vessels, sweat glands, etc. are marked [3].

The outermost part, the epidermis, is composed from the bottom to the top of: stratum basale, stratum spinosum, stratum granulosum, stratum lucidum, stratum corneum [4]. In the epidermis there are up to 90 % keratinocytes, but also melanocytes, Langerhans and Merkel cells, which are responsible for the function of physical, chemical/biochemical and adaptive immunological barriers of the epidermis [5,6].

The basement membrane zone (BMZ) builds up the dermal-epidermal junction (DEJ) to connect the epidermis with the dermis and additionally serves as a multiprotein complex for dynamic interface [7]. The DEJ plays an important role in metabolic exchange between epidermis

and dermis, is involved in immunological and inflammatory processes within the skin and is crucial for migration of keratinocytes and other cells needed for wound healing etc. Basal keratinocytes together with their hemidesmosomes build up one of the four dermal-epidermal junction layers. Lamina lucida, lamina densa and the sublamina densa, which mainly consists of anchoring fibrils, represent the other three BMZ layers [2].

The dermis consists mainly of collagen producing fibroblasts, connective tissue and blood vessels. Additionally, the collagenous elastic structure gives the skin tear strength and plasticity. The dermis can be further separated into stratum papillare and stratum reticulare. The stratum papillare is responsible for mechanical, nutritive, sensory and immunological functions. The stratum reticulare below is a high-fibre connective tissue layer containing a modicum of cells [4]. Nerves, epidermal derived appendages, macrophages, mast cells, different kinds of blood derived cells and fibroblasts as the main cell type are located in the dermis [6].

Underneath the dermis the hypodermis is located, which connects the skin with the subjacent muscles in a relocatable way [4]. The hypodermis comprises mainly adipocytes and furthermore functions as thermo regulator, insulator, storehouse of energy and as protector against mechanical injuries [2].

1.2 Epidermolysis bullosa

Epidermolysis bullosa (EB) is a severe inherited blistering disease affecting the human skin, mucous membranes and different organs. Subsequently to slightly mechanical liability, blisters are formed due to skin separation. This leads to enormous pain for the patients and chronic wounds. Besides skin fragility, easily inducible blister formation and erosion in the skin, also milia, nail dystrophy or total absence of nails, scarring, exuberant granulation tissue, localized or confluent keratoderma of the palms and soles and dyspigmentation are additional symptoms for EB. Non-specific cutaneous findings are decreased or absent hair, albopapuloid lesions and hypo- or hyperhidrosis, which are uncommon symptoms for EB. The state of symptoms, so the absence or presence of them, may be age dependent [8].

The National Epidermolysis bullosa Registry in the United States reports 50 cases of EB per 1,000,000 live births. 92 % of these cases are epidermolysis bullosa simplex, 5 % dystrophic EB, 1 % junctional EB and 2 % are unclassified variants [9]. About 500 people in Austria and

about 30,000 people in Europe are suffering from epidermolysis bullosa. The feasibility of epidermolysis bullosa is 1:17,000 and therefore EB belongs to the rare diseases [10].

There are more than 30 subtypes of EB, which are caused by mutations at least in about 18 different genes. These mutations in proteins, important for the structure and the integrity of the skin in the dermal-epidermal junction zone, could result from loss-of-function or total loss of the proteins (for example collagens and keratins) [11].

Concerning the affected skin layer, epidermolysis bullosa is separated in four major groups. Each type or subtype of epidermolysis bullosa is specified by its state of transmission, phenotype, immunohistochemistry and the molecular findings. Blistering and mechanical fragility within the epidermis is a characteristic of epidermolysis bullosa simplex (EBS). The blistering can occur within the basal or suprabasal level of the epidermis determining the EBS subtype. Junctional EB (JEB) is caused by mutations in proteins in the lamina lucida of the basement membrane zone and leads to blistering within this zone of the skin. Blistering within the upper dermis just beneath the lamina densa is caused by mutations within *COL7A1*, leading to the dystrophic subtype of EB (DEB). The Kindler syndrome is characterized by blistering and mechanical fragility within basal keratinocytes and/or within the lamina lucida, lamina densa and below [12].

In Figure 2 and Figure 3 the exact localisation of important affected proteins and their functions in the skin are shown.

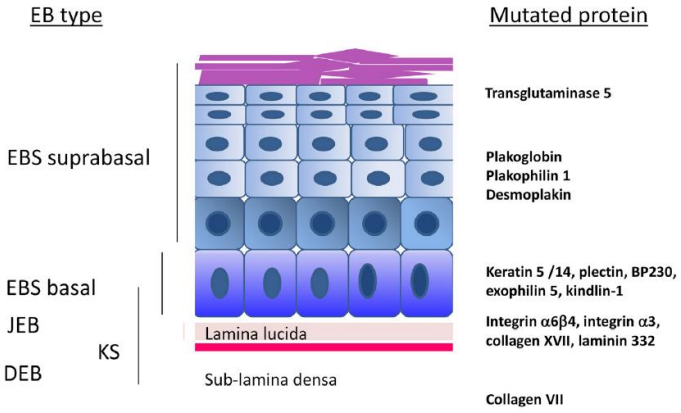

Figure 2. Major groups of epidermolysis bullosa and the relevant mutated proteins in appropriate skin layers. On the left side, the different types of EB and the affected parts of the skin are shown. On the right you can see some of the mutated proteins [12].

For diagnosis immunofluorescence antigen mapping (IFM) or transmission electron microscopy (TEM) on new blisters can be performed. By IFM you can identify structural proteins of

the skin by using antigens. Utilizing this method the level of blistering is determined by the presence, absence or reduced expression of the respective structural proteins. Mutation analysis, so-called molecular fingerprinting, is the common way to diagnose the different types of EB [9,12].

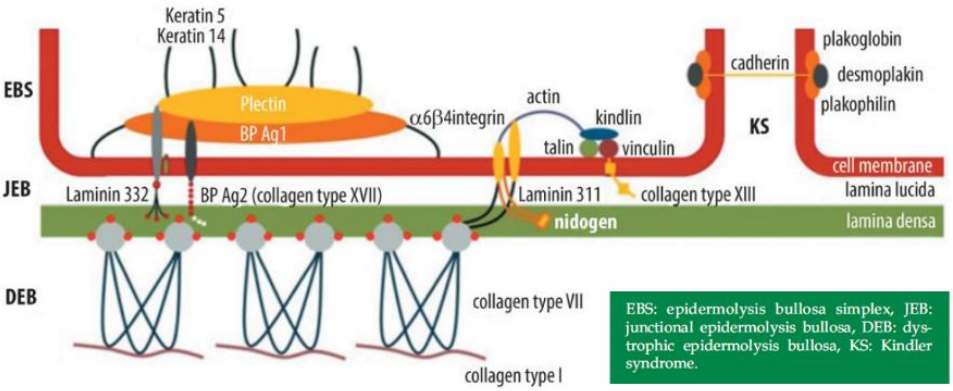

Figure 3. Localisation of mutated proteins in different sections of the skin, causing several epidermolysis bullosa types. This depiction of the skin shows some of the affected proteins, there localisation and natural function in the skin. Additionally the different EB types according to mutated proteins are visualized [9].

1.2.1 Epidermolysis bullosa simplex

The most frequent form of epidermolysis bullosa is EB simplex, which is inherited autosomal dominant. Mechanical stress can induce blister formation and rupture within the basal layer of the epidermis. There are three different types of EBS, namely EBS-generalized (blistering all over the body), EBS-localized (blistering is mainly restricted to hands and feet) and EBS-generalized severe, where blisters show a herpetiform or clustered pattern. EBS-MP (mottled pigmentation) and EBS-MD (muscular dystrophy) are also variants of EBS leading to anomalies in skin pigmentation and are combined with progressive, limb-girdle type of muscular dystrophy [12–14]. Mutations in proteins important for structural purpose in epidermis and related tissue are responsible for EBS. For the mechanical integrity and organization of the cells intermediate filaments, microtubules and microfilaments play an important role. Mutations in *KRT5* and *KRT14* encoding the intermediate filament proteins keratin 5 and 14 cause EBS. Mutations within the gene *PLEC* encoding the cytolinker protein plectin, lead to EBS-MD [13,14]. Figure 4 shows typical blistering of patients, who are suffering from EBS.

Figure 4. Epidermolysis bullosa simplex localized on hand balms and sole of feet [15].

1.2.2 Junctional Epidermolysis bullosa

The autosomal recessive inherited junctional EB, in which genes encoding for proteins within the lamina lucida are affected, can be divided into two forms termed generalized and localized JEB. Mutations in the following genes are the cause of this EB subform: *LAMA3*, *LAMB3*, *LAMC2*, *COL17A1*, *ITGA3*, *ITGA6*, *ITGB4* [12].

JEB patients show a fragility of the skin and mucous membranes and blistering upon minor mechanical stress. The severe blistering and granulation can occur around the oral and nasal cavities, fingers, toes and around the upper airways. There are two subtypes of JEB, the generalized severe and the generalized intermediate JEB [12]. The JEB generalized severe is the more severe variant, in which malformations of urinary tract and bladder are common. An example for the phenotype of the generalized severe form of JEB is shown in Figure 5.

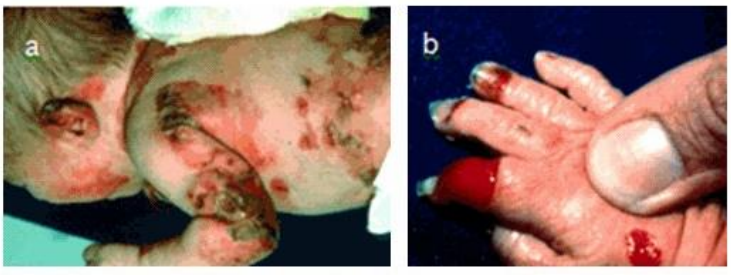

Figure 5. JEB generalized severe of a child showing widespread blistering and granulation [16].

JEB generalized intermediate is the milder variant of JEB and exhibits blisters around the arms, hands, legs and feet [16].

1.2.3 Kindler syndrome

The Kindler syndrome shows a mixed phenotype compared to the other EB types, because the blistering appears in infancy, followed by photosensitivity and progressive poikiloderma, within the basal keratinocytes, in the lamina lucida or below the lamina densa. This autosomal recessive skin fragility genodermatosis is caused by loss-of-function mutations in the gene encoding for kindlin-1 (*KIND1*; also called *FERMT1*), which is expressed in the basal keratinocytes and responsible for the linkage of the actin cytoskeleton to the extracellular matrix [12,17].

1.2.4 Dystrophic epidermolysis bullosa

The dystrophic variant of EB is caused by mutations in the *COL7A1* gene encoding type VII collagen characterized by blisters within the sublamina densa. Patients show reduced number or absolutely absence of anchoring fibrils within the dermal-epidermal junction. A variety of 324 pathogenic identified mutations within *COL7A1* result in diverse and more or less severe forms of DEB [18,19].

The major component of the anchoring fibrils is type VII collagen, which is affected in DEB. This anchoring fibrils connect the basal lamina to the dermal collagen fibrils [18]. Each precursor type VII collagen polypeptide chain consists of an amino terminal non-collagenous (NC-1; from exon 1-28) and a carboxy terminal non-collagenous domain (NC-2; exon 112-118) flanking a central triple-helical collagenous domain. The protein domains NC-1 and NC-2 are essential for the attachment of anchoring fibrils to the basement membrane and for the type VII collagen homotrimers formation (Figure 6). *COL7A1* is located on chromosome 3 and contains 118 exons mainly expressed and secreted from dermal fibroblasts and keratinocytes [20,21].

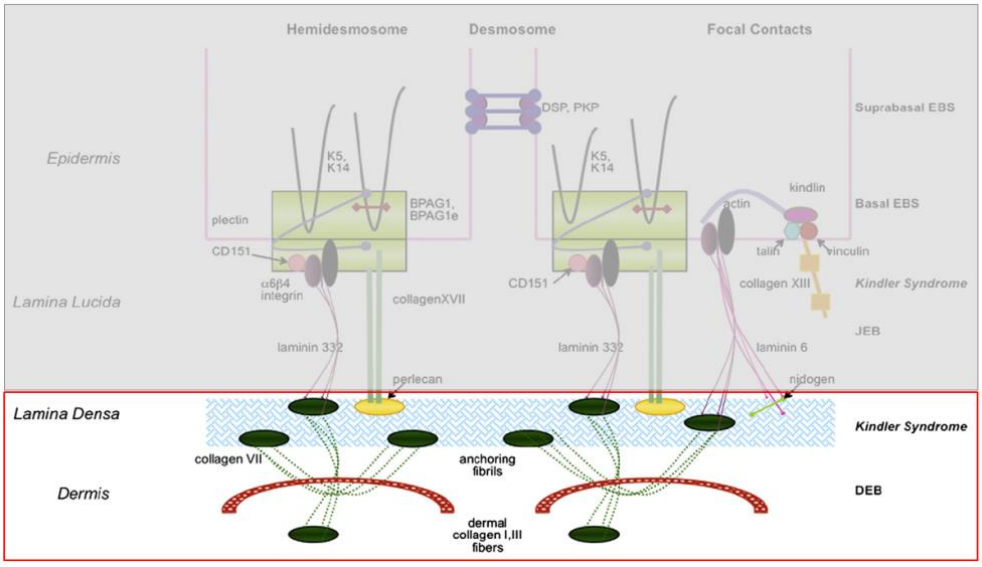

Figure 6. Schema of basement membrane zone and proteins involved in DEB. Inside the red box the anchoring fibrils and type VII collagen as linker of lamina densa and dermis are shown [22].

DEB can be inherited autosomal dominant or autosomal recessive, forming the milder dominant DEB (DDEB) variant or the severe recessive DEB subtype (RDEB). RDEB can be divided into the milder RDEB generalized intermediate and the more severe RDEB generalized severe [12,18].

The dominant inherited DDEB is the second common epidermolysis bullosa subtype and seems to be the milder variant of DEB compared with RDEB. DDEB is mainly caused by glycine substitutions within the triple helical domain of type VII collagen, although also missense, splice site mutations and deletions can lead to the disease [23]. These mutations result in the expression of functionally impacted type VII collagen, destabilizing the triple helix formation [20,22]. The patients suffer from trauma induced generalized blistering, resulting in scarring, milia formation and nail dystrophy [22].

RDEB is caused by missense or nonsense mutations at both *COL7A1* alleles. The more severe form RDEB, generalized severe, is caused by two premature termination codons in *COL7A1* leading to the complete loss of type VII collagen and thus no anchoring fibrils formation within the BMZ. RDEB generalized severe patients show generalized blistering since childbirth, extreme scarring and pseudosyndactyly (mitten deformities of hands and feet) (Figure 7).

Figure 7. RDEB generalized severe patient with pseudosyndactyly (left) and massive generalized blistering (right) [22].

Also mucous membranes are affected; malnutrition, slowed growth, joint contractures and eye inflammation can be other secondary manifestations. Additionally, with progression of age the risk for the development of life-threatening squamous cell carcinoma (SCC) is significantly increased [21].

Mutations, inducing the milder RDEB generalized intermediate variant, are often combined heterozygous inherited. Type VII collagen can be still formed, but the number of anchoring fibrils is significantly reduced. The blistering can be localized or generalized with less/no mitten formation and less frequent extra-cutaneous involvement [18].

1.3 Therapeutic strategies for DEB

Causal therapies for the dystrophic form of epidermolysis bullosa are not available at the moment, but gene and cell therapies are promising tools to antagonize the for DEB causative mutated type VII collagen. Different gene-, cell-, protein- and bone marrow transplantation therapies as well as *trans*-splicing approaches are pursued for the restoration of *COL7A1*, the gene encoding type VII collagen.

Wagner *et al.* (2010) treated 6 children, who suffered from RDEB, with allogeneic stem-cells by bone marrow transplantation. One patient died, because of a graft rejection and infection. The remainders showed a reduction in blister formation, revised wound healing and an increased amount of type VII collagen at the basement membrane zone, however no normalization of the anchoring fibrils could be detected. Additionally, a notably amount of donor cells was seen in children's skin, where no anti type VII collagen antibodies could be detected [24].

A protein-based therapy for DEB was examined by injection of human recombinant type VII collagen into mouse skin and human skin equivalents transplanted onto mice. This therapy resulted in type VII collagen localizing to the basement membrane zone and organizing in anchoring fibrils. Furthermore the features of DEB were reversed [25]. Remington *et al.* (2008) injected human type VII collagen intradermally into DEB mice. This injected human type VII collagen localized to the mouse basement membrane zone, made up anchoring fibrils and decreased DEB features like skin fragility, blister formation and prolonged the survival [26].
Another group transferred type VII collagen using a retroviral vector to dog and human RDEB keratinocytes and they showed a sustained and permanent expression of the transgene product. Hypermotility and the noticeable defects caused by RDEB keratinocytes in cell culture and *in vitro* reconstructed skin were reversed by the recombinant canine type VII collagen in human and canine RDEB keratinocytes [27].
In an *in vivo* gene transfer Sat *et al.* (2000) demonstrated a successful and stable expression of human type VII collagen in transgenic mice. They used a cosmid clone containing the human *COL7A1* gene and showed the localization of this human type VII collagen at the basement membrane zone of the transgenic mice [28]. Woodley *et al.* (2004) demonstrated an efficient and long-term type VII collagen gene transfer *in vivo* by the intradermal injection of a self-inactivating lentiviral vector expressing human type VII collagen into hairless, immunodeficient mice and into human DEB skin equivalent grafts onto such mice. This type VII collagen adhered and incorporated into the basement membrane zone and formed anchoring fibrils between the dermis and epidermis [29].
Ortiz-Urda *et al.* (2002) established an approach for nonviral genetic correction of RDEB. Therefore they used the C31 bacteriophage integrase to stably integrate the large *COL7A1* sequence into genomic *attP* sites of primary epidermal progenitor cells from four unrelated RDEB patients. As a consequence of this nonviral strategy, type VII collagen expression, formation of anchoring fibrils and dermal-epidermal cohesion occurred [30]. On the basis of the publication of Baldeschi *et al.* (2003) the same group showed the full phenotypic reversion of primary RDEB epidermal clonogenic cells mediated by recombinant retroviral vectors carrying the human collagen type VII cDNA [31].
Titeux *et al.* (2010) used a minimal self-inactivating retroviral vector carrying the *COL7A1* cDNA, which was under control of a human promoter, and showed *ex vivo* genetic correction

of RDEB keratinocytes and fibroblasts. These genetically corrected cells were used for the generation of human skin equivalents, which were grafted onto immunodeficient mice. Subsequently they demonstrated *in vivo* functional correction by the long-term expression of type VII collagen with localization at the basement membrane zone and formation of anchoring fibrils [32]. Siprashvili *et al.* (2010) showed the restoration of type VII collagen in immunodeficient mice by using a retroviral vector containing an epitope-tagged *COL7A1* cDNA, which led to the correction of RDEB disease features [33].

Goto *et al.* (2006) transduced DEB keratinocytes and fibroblasts with a particular retroviral vector containing *COL7A1* and transplanted them into nude rats. Interestingly, the transferred fibroblasts supplied a higher amount of collagen VII able to build proper anchoring fibrils to the new basement membrane zone than the transferred keratinocytes. So this group suggested that fibroblasts may be a better target for gene therapy of dystrophic epidermolysis bullosa than keratinocytes [34].

Intradermal injection of normal human or gene-corrected RDEB fibroblasts combined with RDEB keratinocytes led to a restoration of type VII collagen expression at the dermal-epidermal junction *in vivo* in mice. Therefore, these fibroblasts were able to solely produce type VII collagen at the basement membrane zone in RDEB skin [35]. Wong *et al.* (2008) intradermally injected allogeneic fibroblasts to RDEB patients and they noted an increased type VII collagen deposition at the basement membrane zone and an increased formation of anchoring fibrils, although none of these had normal morphology [36]. Fritsch *et al.* (2008) showed by intradermal injection of wild-type fibroblasts into type VII collagen hypomorphic mice a neodeposition of type VII collagen at the basement membrane zone and a viable recovery of the dermal-epidermal junction [37]. Another study demonstrated the increase of the initial rate of erosion healing in RDEB subjects within the first 28 days but not thereafter by single intradermal injection of allogeneic fibroblasts. [38]. Tolar *et al.* (2014) showed the expression of functional type VII collagen in revertant RDEB keratinocytes and theirs reprogramming into induced pluripotent stem cells and therefore this is the start for autologous cellular therapies using “natural” gene therapy in RDEB [39].

Chamorro *et al.* (2016) combined the donor template DNA and a transcription activator-like nuclease (TALEN) in adenoviral vectors, which were transduced into RDEB patient keratinocytes and thereafter led to a high frequency of homology-directed repair (HDR) of a certain

RDEB causing homozygous mutation. Transduction of RDEB keratinocytes with TALEN in absence of the donor DNA led to indel generation due to non-homologous end joining (NHEJ) in proximity of the mutation site. Some of this indels restored the reading frame of *COL7A1.* Anyway, both HDR and NHEJ regenerated the skin in RDEB keratinocytes by the restoration of type VII collagen and his localization at the basement membrane zone [40]. By using TALEN Osborn *et al.* (2013) demonstrated the correction of *COL7A1* gene mutation in primary fibroblasts that were subsequently reprogrammed into inducible pluripotent stem cells (iPSCs). These cells showed a normal protein expression and deposition in a teratoma-based skin model *in vivo* [41]. Also Sebastiano *et al.* (2014) showed the reprogramming of RDEB keratinocytes using adenovirus-associated viral genome editing to generate iPSCs for the treatment of RDEB [42].

Most gene therapy approaches are focusing on the transfer of the full-length *COL7A1* (9 kb) into RDEB cells. But there is a main risk of genetic rearrangements of the large repetitive cDNA sequences. Also the size of the full-length cDNA pushes the envelope of the cloning capacity of viral vector used to transduce affected keratinocytes or fibroblasts, what can result in an instable integration of *COL7A1* in viral vectors. Furthermore, unsolved problems arise with unregulated overexpression and ectopic expression of type VII collagen.

To break through these disadvantages, experts tried to reduce the size of *COL7A1* cDNA for the correction of mutated *COL7A1* by using RNA *trans*-splicing approaches. Murauer *et al.* (2011) had succeeded in the correction of the 3' part of *COL7A1* by 3' *trans*-splicing. RTM transduced keratinocytes showed normal morphology and the expression of full-length type VII collagen localizing at the dermal-epidermal junction and forming functional anchoring fibrils in skin equivalents [43]. One risk in the application of retroviral vectors to transduce affected cells is their potential for genotoxicity due to random integration of the transgene into the genome [44]. To circumvent this concerns Peking *et al.* (2016) established a novel *in vivo* non-viral RNA therapy approach to reprogram murine *Col7a1* via 5' *trans*-splicing [45].

In this work we present the combination 3' and 5' *trans*-splicing in a double RNA *trans*-splicing approach to exchange certain internal mutated exons in *COL7A1* of RDEB keratinocytes.

1.4 General RNA splicing process

In recent years a diversity of gene therapeutic applications came into the clinic. However, besides cDNA substitution strategies, RNA repair strategies have been developed as promising alternatives to conventional gene therapy strategies. RNA *trans*-splicing can be an elegant way to exchange mutated gene parts by the wild-type sequence of the gene, thereby restoring gene function[46,47].

During the expression of eukaryotic genes primary RNA transcripts are generated termed pre-messenger RNAs (mRNAs). These pre-mRNAs contain exons, carrying the genetic information for the protein expression, and introns carrying non coding information. In case of *cis*-splicing, which is executed by an enzymatic complex called spliceosome, the intronic sequences get removed from the pre-mRNA and the exons are assembled to form the mature mRNA. This enzymatic complex consists of many different proteins and four small ribonucleoprotein particles (snRNPs), U1, U2, U5, and U4/U5 snRNPs [47,48].

The splicing process between two particular pre-mRNA molecules is termed RNA *trans*-splicing and is also executed by the spliceosome. For accurate splicing the presence of a donor and acceptor splice site, a branch point sequence and a polypyrimidine tract are required. Additionally, exonic and intronic splicing enhancers (ESEs and ISEs) or/and exonic and intronic silencers (ESSs and ISSs) are involved in the *cis*- or *trans*-splicing process [48,49]. In nature *cis*-splicing occurs far more frequent than *trans*-splicing. In Figure 8 the differences between *cis*- and *trans*-splicing are shown.

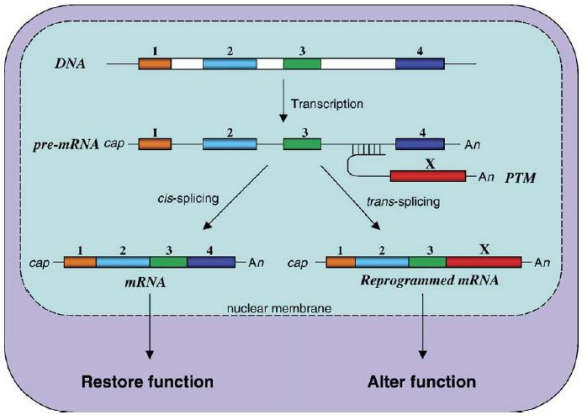

Figure 8. Schematic illustration of cis- and trans-splicing. A pre-mRNA trans-splicing molecule (PTM) induces the trans-splicing event [47].

1.4.1 Spliceosome-mediated RNA *trans*-splicing

Spliceosome-mediated RNA *trans*-splicing, in short SMaRT, is a natural process, where the exons of two or more particular pre-mRNAs are linked to build a new RNA molecule. SMaRT is an elegant method to correct genetic diseases, such as epidermolysis bullosa, cystic fibrosis and others [43,46,50].

For the *trans*-splicing reaction at least two different RNA molecules have to be available for the spliceosome, in particular an RNA *trans*-splicing molecule (RTM) and a second RNA molecule as target for the RTM. The main composition of an RTM comprises i) a binding domain which is complementary to the target intron sequence and guide the RTM to a specific location in the target sequence, ii) a splicing domain which contains several important elements that are equivalent to *cis*-acting elements; and iii) a coding domain consisting of these exons that should be combined with the target. Except for the coding domain, the binding and splicing domain are not part of the newly generated chimeric RNA molecule [47,51].

The composition and the characteristics of the RTM's binding domain (BD) plays a critical role in the *trans*-splicing process. Koller *et al.* (2014) noted some important features in the design of BDs. Besides the length and the GC content of the BD, the binding position plays a crucial role the interaction of RTM and target [52]. Amongst others the binding domain is accounted for the specificity between the RTM and the target mRNA in the *trans*-splicing process [47].

The *trans*-splicing process needs several significant splicing elements in the splicing domain of the RTM, which can be also found in *cis*-splicing. 5' donor and 3' acceptor splice sites acting as the boundary sequence between exons and introns. The branch point (BP), adenosine composition, is located upstream of the 3' acceptor splice site and at least a polypyrimidine-rich sequence called polypyrimidine tract (PPT), just before the 3' splice site, is required for a proper RTM splicing domain. The coding sequence contains the cDNA or particular exons for the substitution of the target's sequence. Figure 9 visualises the important domains of an RNA *trans*-splicing molecule [53]. Anyway, the design of an RTM is very significant for a specific efficient *trans*-splicing event.

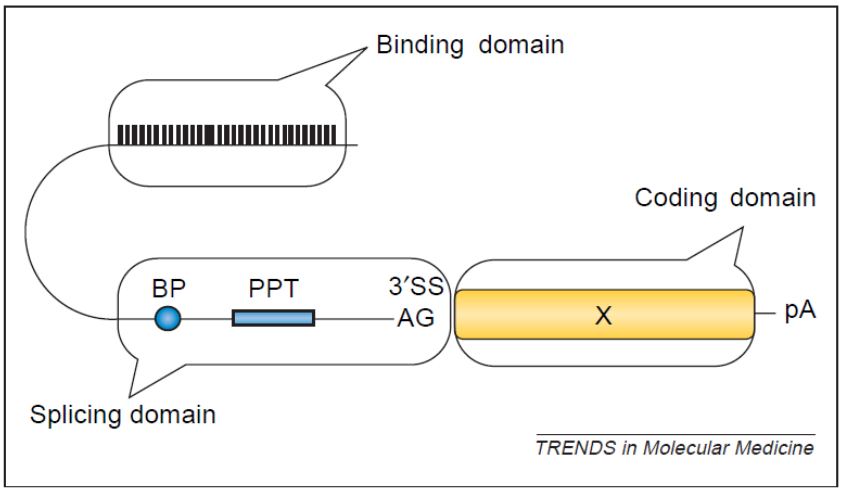

Figure 9. Schematic representation of the important domains within an RNA *trans*-splicing molecule (RTM). The main components of an RTM are the binding domain, essential splice elements for efficient splicing (splicing domain) and the coding domain containing the sequence for the substitution. BP = branch point, PPT = polypyrimidine tract, SS = splice site, pA = poly A signal; [51]

Trans-splicing occurs between two or more different RNA molecules by two *trans*-esterification reactions, where splicing elements like BP and PPT play a crucial role (Figure 10).

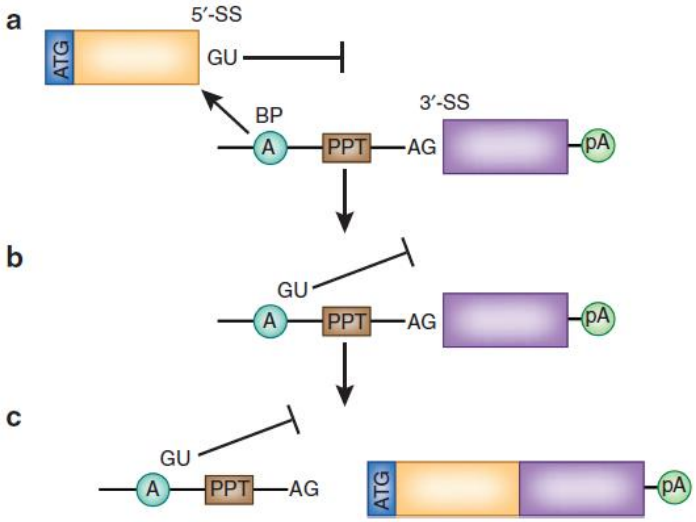

Figure 10. Two *trans*-esterification reactions occur during *trans*-splicing. (a) Step 1, the 2'-OH group from the adenosine residue of the branch point attacks the phosphoryl group of the 5' target splice site. (b) The 5' exon is released and the 5' end of the RTM builds a Y-branched structure. Now the 3' OH of the 5' exon attacks the phosphoryl group of the 3' splice site. (c) Afterwards the 5' target exon can join the RTM exons and a new chimeric RNA molecule was generated. PPT and 3' AG are critical for the initial identifying of an intron. BP = branch point, PPT = polypyrimidine tract, pA = poly A signal, SS = splice site

As described by Wally *et al.* (2012) RNA *trans*-splicing can act in three different ways, depending on the target sequence to be exchanged: i) 5' *trans*-splicing, ii) 3' *trans*-splicing and iii) internal exon replacement also called double *trans*-splicing. According to that, the RTM design is different for these three applications (Figure 11) [54].

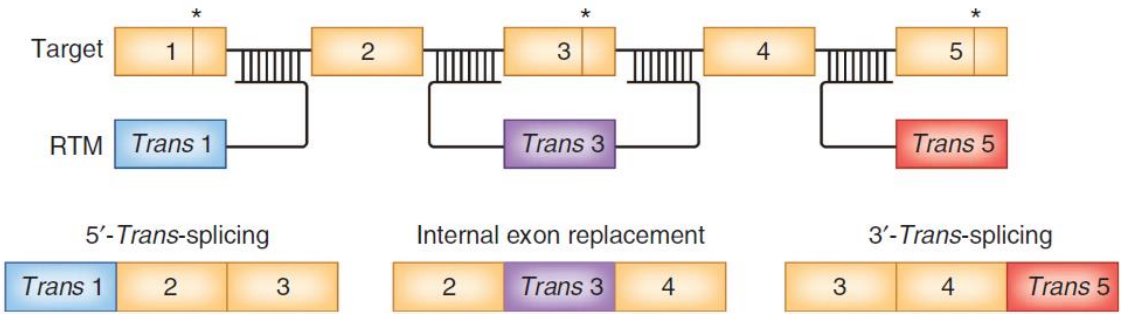

Figure 11. Spliceosome mediated RNA *trans*-splicing replaces either 5', 3' or internal exons of a gene, termed 5' *trans*-splicing, 3' *trans*-splicing and internal exon replacement (double *trans*-splicing). Upon accurate *trans*-splicing the mature messenger RNA (mRNA) consists of the particular wildtype coding sequence derived from the RNA *trans*-splicing molecule (RTM) (*Trans* 1, *Trans* 2, *Trans* 3) and the residuary exons of the target sequence. * displays mutations in the exons of the target mRNA to be replaced [54].

In case of 5' RNA *trans*-splicing the 5' part of the target pre-mRNA gets exchanged, in contrast to the replacement of the 3' section of the target molecule (3' *trans*-splicing). For 5' *trans*-splicing the RTM lacks of BP and PPT in the splicing domain. A start codon has to be included at the 5' end of the RTM to ensure a proper expression of the respective protein (Figure 10). If a gene part in the middle of the target molecule gets replaced, double RNA *trans*-splicing occurs [54]. The double RNA *trans*-splicing molecule is a combination of 5' and 3' RTM and contains two binding domains, a 3' SS (including BP, PPT) and 5' SS (splice site) (Figure 12).

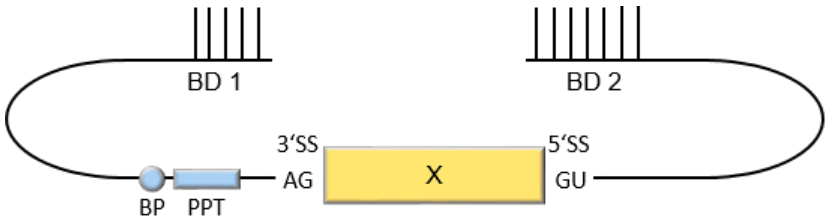

Figure 12. Schematic view of an RTM for double *trans*-splicing. The 3' splicing domains contains important splicing elements like branch point (BP) and polypyrimidine tract (PPT). The 5' splice site (SS) does not need the BP and PPT elements. To be able to bind upstream and downstream of the exons to be exchanged, the double RNA trans-splicing molecule (dRTM) requires two different binding domains. X displays the coding sequence for the substitution of the target exons.

The power of *trans*-splicing to modify genes at pre-mRNA level in view of therapeutic aspects in different genetic diseases has been shown by different groups using 3', 5' and double RNA *trans*-splicing strategies.

There are some reports on the correction of gene function using 3' *trans*-splicing. For example Murauer *et al.* (2011) showed the correction of RDEB causing mutations in type VII collagen encoding gene *COL7A1* using 3' *trans*-splicing *in vitro*. Therefore RDEB keratinocytes were retrovirally transduced with the 3' RTM leading to an increase of *COL7A1* mRNA detected by

SqRT-PCR and the restoration of full-length *COL7A1* expression validated via western blotting and immunofluorescence staining. Corrected RDEB keratinocytes showed normal morphology, a normal localization of type VII collagen at the basement membrane zone and formation of anchoring fibrils in skin equivalents [43]. Also Philippi *et al.* (2015) rescued mutated dysferlin, which is responsible for muscular dystrophy (limble girdle muscular dystrophy 2B; Miyoshi muscular dystrophy 1), using the 3' *trans*-splicing approach. Different from previous SMaRT strategies, they focused on the identification of suitable target introns other than optimization of the 3' RTM. They demonstrated that the target intron containing weakly defined 3' SS was *trans*-spliced successfully both *in vitro* and *in vivo* [55]. RDEB patients have a high risks to develop highly aggressive squamous cell carcinoma (SCC). Gruber *et al.* (2011) used a 3' RTM to *trans*-splice a suicide gene into a tumor marker gene of RDEB SCC cells. They showed the insertion of streptolysin O into tumor marker gene *MMP9* in RDEB SCC by 3' *trans*-splicing, which resulted in cell death and induction of toxin function predominantly in RDEB SCC [56]. Coady *et al.* (2010) demonstrated that the *trans*-splicing of *Survival Motor Neuron-2* (*SMN2*), associated with spinal muscular atrophy (SMA), in combination with an antisense RNA strategy leads to a reduction of the severity of the SMA phenotype and an extension of survival of about 70 % in mice *in vivo* [57]. Another group managed to mediate *trans*-splicing of human apolipoprotein A-I (hapoA-I) into highly abundant mouse albumin transcripts by 3' *trans*-splicing. Therefore they injected the hapoA-I RTM by hydrodynamic tail vein injection in mice and checked the occurred *trans*-splicing by detection of the chimeric mRNA product and the production of hapoA-I protein. So at least Wang *et al.* (2009) demonstrated that *trans*-splicing into highly abundant albumin transcripts is a good tool to produce therapeutic proteins *in vivo* by also producing functional human papillomavirus type-16 E7 single-chain antibody in C57BL/6 mice and functional factor VIII (FVIII) and phenotypic correction in hemophilia A mice [58]. Chen *et al.* (2009) showed the correction of the mutated dystrophia myotonica protein kinase (DMPK), which causes dystrophia myotonica type 1 (DM1), by using 3' *trans*-splicing molecules in human myosarcoma cells (CLL-136) [59].

Not only 3' *trans*-splicing but also 5' *trans*-splicing was applied for the repair of various genetic disorders. Peking *et al.* (2016) recently published a 5' *trans*-splicing approach to correct mutations in *COL7A1*, leading to recessive epidermolysis bullosa. Reprogramming of *Col7a1* by 5' *trans*-splicing was confirmed in murine keratinocytes, both *in vitro* and *in vivo*. Therefore a

minicircle plasmid, expressing a 3x FLAG tagged 5' *trans*-splicing molecule, was delivered into the skin of wild-type mice via gene gunning. The *trans*-splicing product was then detectable via western blot analysis and immunofluorescence staining using a FLAG tag specific antibody [45]. Mearini *et al.* (2013) demonstrated the power of 5' *trans*-splicing by correction of mutations in *MYBPC3*, encoding cardiac myosin-binding protein C mRNA. Mutations in *MYBPC3* lead to the cardiac autosomal dominant disease hypertrophic cardiomyopathy (HCM). They showed the full-length repaired Mybpc3 transcript and the restored protein both in cultured cardiac myocytes and in the heart *in vivo* [60]. A mutation in exon 1 of the keratin 14 gene (*KRT14*) causes the autosomal dominant disease epidermolysis bullosa simplex-type Dowling-Meara (EBS-DM). Wally *et al.* (2010) published the correction of mutated *K14 in vitro* in an EBS-DM patient cell line on RNA and protein level by the use of a highly efficient 5' RTM confirming *trans*-splicing to be a promising tool for the treatment of autosomal dominant inherited genetic diseases [61]. Additionally, the same group succeeded in the correction of mutated *PLEC* gene by a transient transfection of a 5' RTM carrying the 5' wild-type portion of *PLEC* cDNA into EBS-MD fibroblasts, resulting in increased wild-type *PLEC* expression levels. Kierlin-Duncan *et al.* (2007) established a 5' RTM to repair the 5' end of mutant ß-globin transcripts involved in sickle cell anemia and ß-thalassemia. They co-transfected mutant genomic ß-globin DNA and specific 5' RTMs in HEK293T cells and detected occurred *trans*-splicing on mRNA level by one step RT-PCR [62]. The therapeutically benefit of 5' *trans*-splicing for human diseases was also shown by Mansfield *et al.* (2003) demonstrating the correction of the mutated gene encoding the cystic fibrosis transmembrane receptor CFTR. They performed a co-transfection of a mutant minigene target and a 5' RTM into HEK293T cells and detected a consistent increase in anion efflux transport in the cells [63].

By combining 5' and 3' *trans*-splicing internal parts of genes can be exchanged by internal exon replacement also termed double RNA *trans*-splicing. The benefit of this *trans*-splicing strategy, compared to 3' and 5' *trans*-splicing, is the ability to exchange individual exons within the gene. Lorain *et al.* (2010) demonstrated the functionality of this approach using a dystrophin minigene, carrying mutated exons of the *mdx* dystrophin gene, for the first time [64].

One benefit of RNA *trans*-splicing in gene therapy is the possibility to correct multiple mutations by using one RNA *trans*-splicing molecule (RTM) in contrast to other technologies (e.g.

CRISPR). Another advantage is the aspect that in general the RTM is inert except for the *trans*-splicing reaction. So there is physiological natural regulation of the newly generated chimeric RNA depending on the natural regulation of the targeted pre-mRNA. This is crucial for gene therapy, where the expression of genes has to be kept on a defined physiological level. An RTM can reduce the expression of the mutated gene accompanied with the increase of wild-type expression levels. In contrast to other approaches RNA *trans*-splicing only requires one molecule, the RTM, to correct mutations in a gene. The other required components (target pre-mRNA and spliceosome) are already naturally present in the cell. There are often limitations, because of the size of the transgene, in the choice of retroviral vectors. For RNA *trans*-splicing only a part of the full-length cDNA is needed for the correction of mutations and therefore the viral vector choice is enlarged [53].

The mechanism of *cis*-splicing is well understood and the knowledge is anchored in the literature, but about the *trans*-splicing process there are some black holes left. This lack in knowledge about *trans*-splicing make it difficult to e.g. predict the efficiency and the secondary structure of a particular RTM. Furthermore the isolation of the *trans*-splicing products is fatally more complicated than those occurred from *cis*-splicing [53]. Interestingly Philippi *et al.* (2015) reported the importance not only of the RTM but also of the target intron sequence regarding *trans*-splicing efficiency [55]. Off-target effects with random pre-mRNAs are also possible and therefore several approaches should be minded. The binding domains of the RTM with complementary sequences to the target should have a particular length to both increase the specificity of the RTM and to maintain a good *trans*-splicing efficiency. Experts demonstrated the increase of RTM efficiency by binding domains up to a length of 153 bp [65]. Additionally, the amount of RTM in the target cell is a crucial factor for the *trans*-splicing efficiency as Berger *et al.* (2015) reported [66]. So a big drawback in SMaRT is the design of RTM revealing a high specificity for the target region and inducing a highly efficient *trans*-splicing reaction. Koller *et al.* listed the advisements about the design of highly functional RTMs considering the selection of *trans*-splicing reactions, planning and preparation of the screen using their developed screening system, selection of binding domains, design of endogenous RTMs and the choice of vectors for the delivery [52,67]. One of the major problems occurring in *trans*-splicing is the low efficiency compared to the *cis*-splicing reaction. Berger *et al.* (2016) assume that

the knowledge to define the rules to get 100 % reaction efficiency, while guarantying the absence of off-target effects, would make of the SMaRT technology an inconceivably effective and powerful gene therapy tool [53].

1.5 Fluorescence-based RTM screening system

Koller *et al.* (2011) and Wally *et al*. (2011) showed in recent studies the significance of binding domain design regarding RNA *trans*-splicing [67,68]. Considerations for the design of optimal RNA *trans*-splicing molecules for RNA repair were published by Koller *et al*. in 2014 [52]. The efficiency of RNA *trans*-splicing depends on the length, composition and localization of the binding domain. Besides Philippi *et al.* (2015) additionally showed the importance of 3' splice site strength in target introns on the 3' *trans*-splicing-mediated correction of *DYSF* encoding dysferlin. They demonstrated an increase of 3' *trans*-splicing by the presence of target introns containing weak 3' splice sites [55].

For the identification of functional RTMs carrying highly efficient binding domains (BDs) Bauer *et al.* (2013) published a reporter-based screening system [69]. In this system a target independent RNA *trans*-splicing molecule (RTM) backbone is included. Binding domains for specific target binding are generated randomly and cloned into the RTM backbone. This specific target region consists of the exonic region, which should be exchanged, and the neighbouring introns. To select highly efficient BDs this target region is fragmented randomly by sonification and cloned into the RTM backbone. A fluorescence reporter, in this case full-length green fluorescence protein (acGFP), is building the coding region of the RTM. This acGFP is split into two (3' and 5' *trans*-splicing) or three parts (double *trans*-splicing). The RTM can carry another fluorescence reporter as transfection control (DsRED) (Figure 13). The fragmented target region is cloned into the RTM backbone and so an RTM library with high BD diversity is generated. For the identification of functional BDs individual RTMs of the RTM library are transfected into cells, which must not endogenously express the gene of interest, together with an artificial target molecule carrying the targeted exon/intron region, functional splicing domains and the remaining portion of the reporter molecule acGFP. Prior to this co-transfection cryptic *cis*-splice sites within the target should be removed by mutagenesis to prefer the *trans*-splicing event. After co-transfection of an individual RTM and the target molecule, a restoration of the fluorescence reporter is happening, which can be detected by flow cytometry (Figure 13). The

ratio between this fluorescence signal and the signal of the other fluorescence reporter for the transfection efficiency shows the functionality of the binding domains. As highly efficient selected binding domains could now be characterized by sequence analysis and cloned into a RTM for further endogenous studies [69].

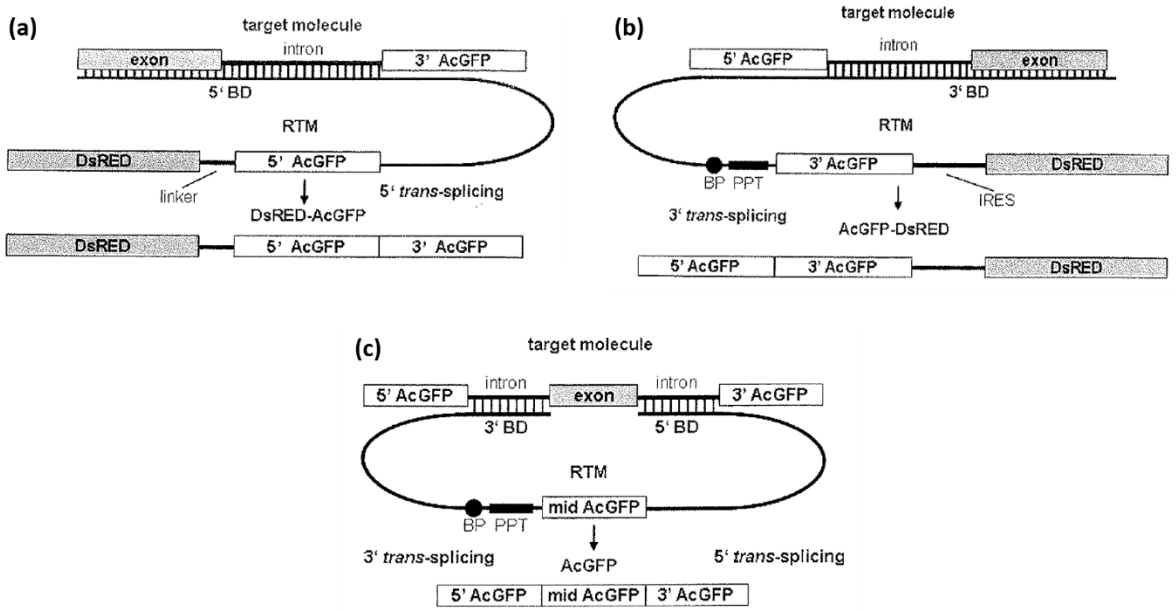

Figure 13. Schematic depiction of the *trans*-splicing screening constructs. The fluorescence reporter was split into two parts for the screening of functional binding domains for **(a)** 5' *trans*-splicing and **(b)** 3' *trans*-splicing. In **(c)** the acGFP was separated into three part for the double *trans*-splicing screen. The screening RNA *trans*-splicing molecules (RTMs) can carry a second fluorescence reporter (DsRED) as transfection control. After co-transfection of the target molecule and the appropriate RTM the acGFP is restored and could be detected by flow cytometry [69].

The selection of the efficient double RNA *trans*-splicing molecule (dRTM) 31/1, which was applied in this study, was performed by using this fluorescence-based screening system. The publication of Koller *et al*. (2011) introduces the screening system for dRTMs regarding the repair of mutated exon 52 of *COL17A1* via double RNA *trans*-splicing (Figure 14) [67]. As you can see in Figure 14, the 3' binding domain is complementary to the upstream target intron 51 and the 5' BD is binding to intron 52. If the *trans*-splicing events occur between the target molecule and the dRTM, the 5' acGFP, int. acGFP and 3' acGFP fuse and subsequently the full-length GFP is expressed, which can be detected by flow cytometric analysis or western blotting.

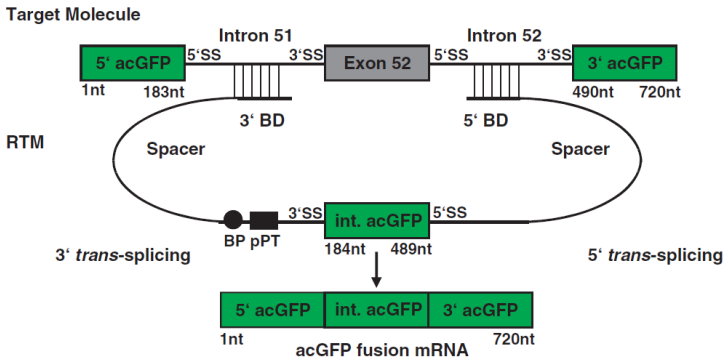

Figure 14. Schematic depiction of fluorescence-based screening model to observe functionality of RNA *trans*-splicing molecules to repair a mutation in *COL17A1* [67].

In order to maintain highly efficient binding domains for 3’ and 5’ *trans*-splicing induction several RTM target regions, flanking the mutated exon 105 of *COL7A1*, were initially selected for the BD screening procedure described by Koller *et al*. (2011) [67]. Thereby a BD for 3’ TS induction specific for intron 102 and a BD for 5’ TS specific for intron 105 were initially selected and incooperated into a double RNA *trans*-splicing RTM. The construction of the dRTM was performed according to Koller *et al.* (2011) [67]. The generation of the *COL7A1*-specific dRTM (dRTM 31/1), used in this study, was performed as recently published [67,69]. The most promising BDs BD 31 [70] and BD 1 (unpublished data) were cloned up- and downstream to the internal GFP part (int. acGFP). The target molecule contains the 5’ and 3’ acGFP part and in the middle intron 102 to intron 105 of mutated *COL7A1.* The co-expression of the dRTM and the target molecule should lead to the expression of full-length GFP restored by correct double RNA *trans*-splicing. The screening plasmids were kindly provided from Dr. Ulrich Koller.

1.6 Improvement of RNA *trans*-splicing using antisense RNAs

Antisense oligonucleotides (ASOs) were used in the past for therapy of spinal muscular atrophy caused by loss of *Survival Motor Neuron-1* (*SMN1*). Patients keep at least one nearly identical gene *SMN2*. *SMN2* is mostly alternatively spliced and *SMN2* exon 7 get skipped [57,71]. Hua *et al.* (2008) designed two ASOs blocking intronic splicing silencers (ISSs) in intron 7, precisely for ISS inhibitory character responsible hnRNP A1/A2 motifs [71]. These ASOs raised the inclusion of human *SMN2* exon 7. Coady *et al.* (2008; 2010) generated antisense oligonucleotides which intensify the alternative splicing of *SMN2* and block competing endogenous *cis*-splice sites to enforce the *trans*-splicing event [57,72].

Antisense strategies were also applied to increase the *trans*-splicing-mediated RNA repair of *COL7A1* in dystrophic epidermolysis bullosa [70]. The inclusion of an antisense RNA, competitive splicing elements of an artificial designed *COL7A1*-minigene led to increased *trans*-splicing of the selected 3' RTM. In order to increase the efficiency of our constructed dRTM we exploited our fluorescence-based screening system to select antisense RNAs capable to further enhance the *trans*-splicing efficiency.

2 Aim of the study – Hypothesis

Due to the lack of a causal therapy for the severe dystrophic variant of the blistering skin disease epidermolysis bullosa several repair strategies for *COL7A1* are currently under development.

COL7A1 has a size of about 8,7 kb and represents a suitable target for the mRNA repair method SMaRT, where exons of two or more different mRNA molecules get combined to build a new reprogrammed mRNA construct. Murauer *et al.* (2011) as well as Peking *et al.* (2016) have successfully demonstrated the replacement of *COL7A1* portions via 3' and 5' *trans*-splicing, respectively [43,45]. In order to significantly reduce the RTM size and to avoid possible side effects maintained by the highly repetitive sequence within *COL7A1* we considered to combine 3' and 5' *trans*-splicing to specifically exchange one or more internal exon(s) within *COL7A1.*

The aim of this study was the detection of successful mRNA repair in RDEB patient keratinocytes treated with the already provided dRTM 31/1, which harbours two functional binding domains (BD 31 and BD 1) specific to the introns flanking the gene region spanning from exon 103 to 105 of *COL7A1*.

The *trans*-splicing efficiency will be investigated in an already established screening model using GFP as reporter for accurate *trans*-splicing and a *COL7A1* target molecule stably or transiently expressed in a HEK293 cell line. Accurate double RNA *trans*-splicing will lead to the restoration of full-length GFP expression in the screening context and more important in the endogenous situation in RDEB keratinocytes to the restoration of type VII collagen upon stable RTM integration into the genome using a retroviral vector.

The second goal of this master thesis was the generation of antisense RNAs capable to increase the double RNA *trans*-splicing efficiency by blocking competitive target *cis*-splice sites. Therefore we exploit the fluorescence-based screening system to accelerate and facilitate the selection of promising antisense RNAs for subsequent experiments in an endogenous model system.

We hypothesize that dRTM 31/1 has the capability to induce double RNA *trans*-splicing, leading to the replacement of mutated exon 105 by its wild-type version manifested in the restoration of a type VII collagen expression in patient cells.

3 Results

3.1 Evaluation of *trans*-splicing efficiency of screening dRTM 31/1

Our primary aim was the analysis of the double RNA *trans*-splicing efficiency of the screening dRTM 31/1, containing the most efficient binding domains BD 31 and BD 1, using our fluorescence-based screening system [67,69,73]. To evaluate the 3', 5' and double RNA *trans*-splicing separately, the dRTM 31/1, carrying the internal acGFP part, was co-transfected with the *COL7A1*-double *trans*-splicing-minigene (*COL7A1*-dTS-MG) into HEK293 cells or in the *COL7A1*-dTS-MG stably-expressing target cell line. *COL7A1*-dTS-minigene is composed of the 5' acGFP part, in between the *COL7A1* gene region spanning from intron 102 to intron 105 of *COL7A1* and the 3' acGFP part.

The combination of 3' and 5' *trans*-splicing leads to the fusion of the internal acGFP part provided by the dRTM to the 3' and 5' acGFP portion of the minigene generating full-length GFP (Figure 15a). The amount of GFP-expressing cells and the intensity of GFP signal detected via fluorescence-activated cell sorting analysis (FACS) within the target cells correlates with the functionality of the generated dRTM.

As shown in Figure 15b co-transfected HEK293 cells revealed a GFP expression of about 15 % in comparison to the with dRTM 31/1-int. acGFP transfected target cell line in which GFP is hardly to detect via flow cytometric analysis.

Additional to the FACS analysis SqRT-PCRs were performed to determine the 3' and 5' *trans*-splicing efficiency in both systems, in the co-transfection system in HEK293 cells and in the single dRTM transfection system in HEK293 cells stably expressing the minigene.

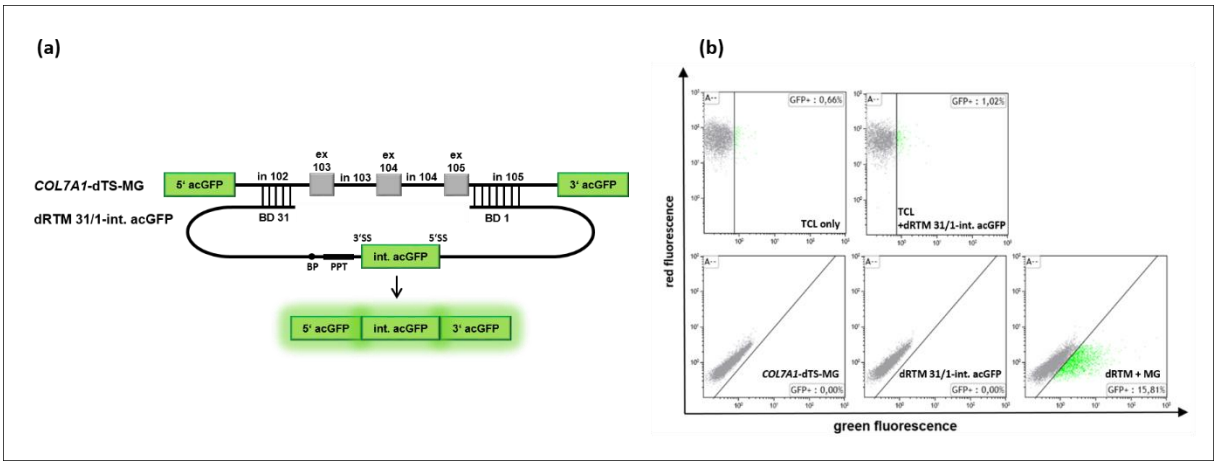

Figure 15. Screening for *trans*-splicing events using the fluorescence-based screening system. a) Schematic representation of the screening system. *COL7A1*-dTS-MG contains 5' and 3' acGFP and *COL7A1* sequence spanning from intron 102 to intron 105. dRTM 31/1-int. acGFP contains the internal acGFP part and BD 1 and BD 31, which have complementary sequences to intron 102 and intron 105, respectively. If double RNA *trans*-splicing occurs, full-length green fluorescence protein is generated. BP = branch point, PPT = polypyrimidine tract, SS = splice site; **b)** According to transfection of the screening dRTM in the *COL7A1*-dTS-MG stably expressing target cell line, GFP expression is hardly detectable. In contrast to that in 15 % of HEK293 cells, co-transfected with dRTM 31/1-int. acGFP and *COL7A1*-dTS-MG, GFP is expressed. TCL = target cell line, MG = minigene, dRTM = double RNA *trans*-splicing molecule

To separately determine both the 5' and 3' *trans*-splicing efficiency induced by dRTM 31/1 in HEK293 cells or in the target cell line on RNA level, we performed semi-quantitative real time PCR (SqRT-PCR) on the total RNA of transfected cells. Therefor we used for the 5' *trans*-splicing detection primers binding to the 5' acGFP part and to the int. acGFP portion. 3' *trans*-splicing was proven by the inclusion of a primer pair binding the int. acGFP and the 3' acGFP part.

Double RNA *trans*-splicing was increased in the co-transfection model compared to the target cell line system similar to the data achieved via flow cytometric analysis. Accessory to that, 5' *trans*-splicing efficiency was higher in comparison to 3' *trans*-splicing in both screening systems as shown in Figure 16a.

This finding is already obvious on the agarose gel after gel electrophoresis showing more intensive 5' *trans*-splicing products in comparison to 3' *trans*-splicing products (Figure 16b). Accurate double RNA *trans*-splicing was confirmed by SqRT-PCR via primers binding the 5' acGFP/int. acGFP and int. acGFP/3' acGFP junction, respectively (Figure 16c, d, e). Similar to the individual splicing reactions (Figure 16a, b) the efficiency of double RNA *trans*-splicing is higher in *COL7A1*-dTS-MG and dRTM 31/1-int. acGFP co-transfected HEK293 cells than in the stable MG cell line treated exclusively with the screening dRTM.

In summary the *trans*-splicing efficiency was higher in the co-transfection HEK293 model than in the stable *COL7A1*-dTS-MG-expressing cell line. Additionally, 5' *trans*-splicing induced by

the screening dRTM 31/1-int. acGFP was far more efficient than 3' *trans*-splicing in both model systems.

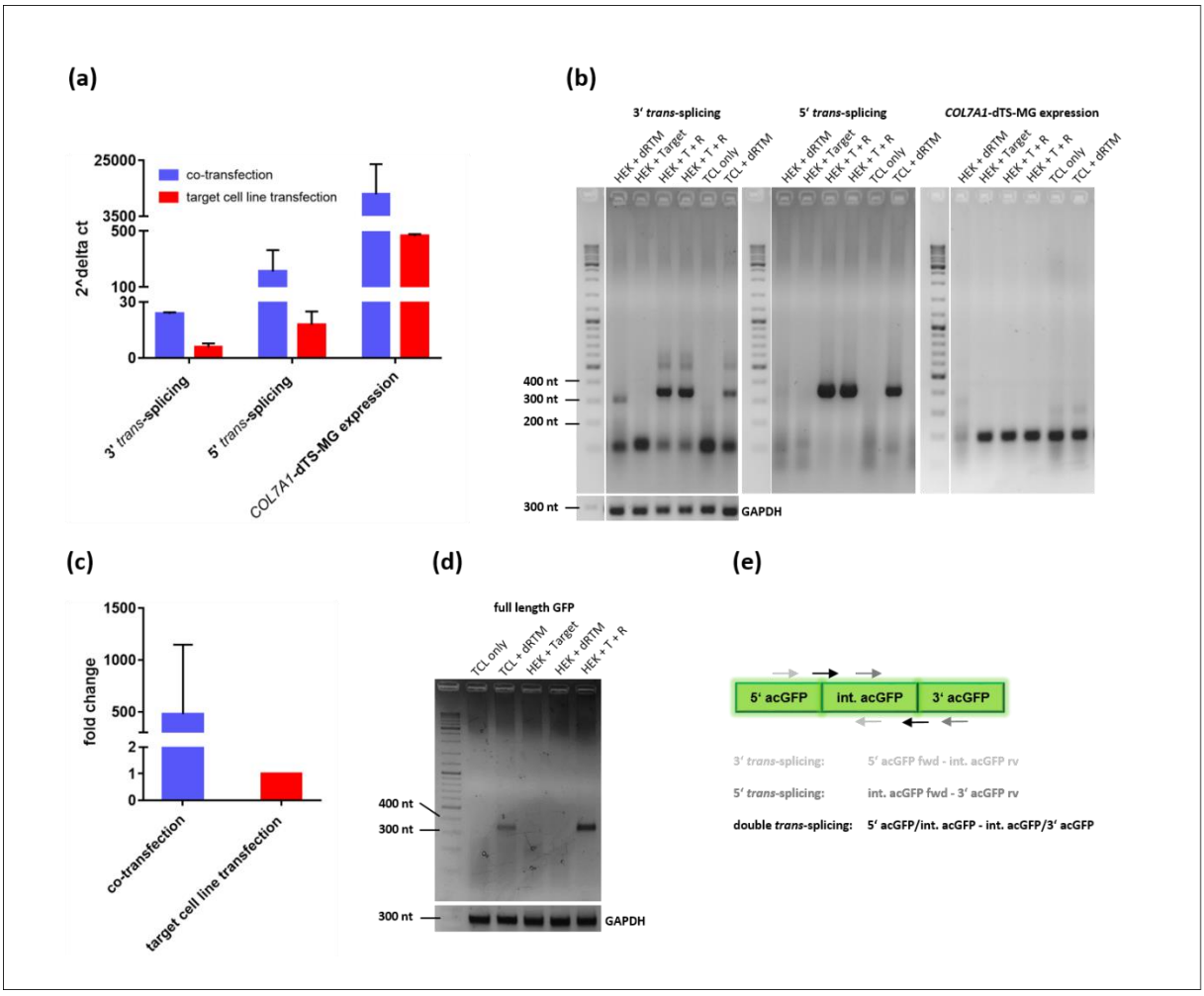

Figure 16. Semi-quantitative analysis of *trans*-splicing efficiency. a) SqRT-PCR on RNA of treated HEK293 cells revealed a higher 5' *trans*-splicing efficiency in comparison to the 3' *trans*-splicing efficiency in regardless if the co- or single RTM transfection system was used. In general the efficiency of both splicing processes is higher in the co-transfection system due to the expression of higher *COL7A1*-dTS-MG amounts as detectable in the target cell line as confirmed by SqRT-PCR analysis. The mean values + SD of two independent experiments are shown. **b)** The 3' *trans*-splicing product appears at a size of 346 nt and the 5 '*trans*-splicing product at 370 nt on the agarose gel after gel electrophoresis. To quantify the *COL7A1*-dTS-MG expression a primer set specific for 5' acGFP portion was included in the SqRT-PCR (171 nt). **c)** To quantify the level of double RNA *trans*-splicing products (full-length GFP) primers binding the junction of 5' acGFP/int. acGFP and int. acGFP/3' acGFP were included in the SqRT-PCR. Double RNA *trans*-splicing efficiency was higher in dRTM, MG co-transfected HEK293 cells in comparison to the dRTM treated HEK293 MG cell line. The mean values + SD of three independent experiments are shown. **d)** The size of the double RNA *trans*-splicing product using primers binding the junction of 5' acGFP/int. acGFP and int. acGFP/3' acGFP is 345 nt. **e)** In total three different primer pairs were used for the quantification of the levels of 3', 5' and double RNA *trans*-splicing.

3.2 Detection of endogenous *trans*-splicing in stably MG expressing HEK293 cells

For endogenous experiments in patient keratinocytes, carrying a homozygous mutation (R2610X) in exon 105 of *COL7A1*, the internal acGFP part of the screening dRTM 31/1-int. acGFP was replaced with the modified *COL7A1* wild-type sequence spanning from intron 102 to intron 105 containing a 3x FLAG tag between exon 104 and exon 105 (Figure 17a). The 3x FLAG tag was inserted to facilitate the detection of accurate RNA *trans*-splicing. Initially the dRTM 31/1-FLAG was transfected into the stable *COL7A1*-dTS-MG expressing target cell line. Accurate 3' and 5' *trans*-splicing products were detected via Reverse Transcriptase-PCR (RT-PCR) on RNA level and confirmed by sequence analysis (Figure 17b, c). The 3' *trans*-splicing product was visible at a size of 317 nt and the 5' *trans*-splicing product at 227 nt on the agarose gel (Figure 17b).

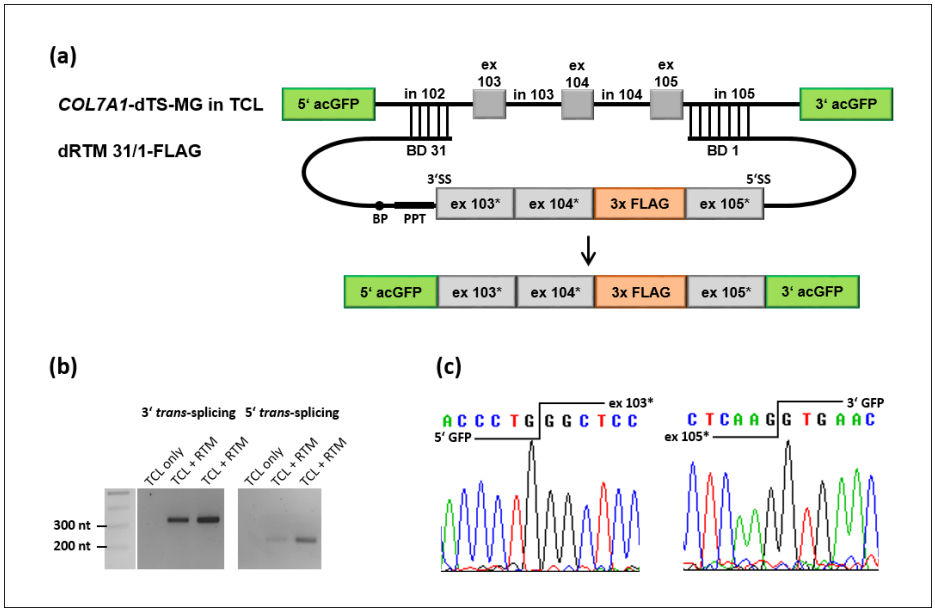

Figure 17. Detection of correct *trans*-splicing in stably *COL7A1*-dTS-MG expressing target cell line. a) Schematic representation of double RNA *trans*-splicing-induced replacement of exon 103-105 of *COL7A1* in the dTS-MG-expressing cell line (TCL). Modified (deleted cryptic splice sites) exons are marked with a *. RTM = RNA *trans*-splicing molecule; **b)** After dRTM 31/1-FLAG introduction (2,5 µg and 5 µg, respectively) in the dTS-MG-cell line RT-PCR on isolated RNA revealed the presence of 3' *trans*-splicing product with a size of 317 nt and 5' *trans*-splicing products with a size of 227 nt. **c)** The junction between 5' acGFP and the modified exon 103 confirmed accurate 3' *trans*-splicing, the fusion of the modified exon 105 and 3' acGFP represents successful 5' *trans*-splicing events. BP = branch point, PPT = polypyrimidine tract, SS = splice site

Subsequently we performed SqRT-PCR to quantify these events and similar to the results in the screening model, there were more 3' and 5' *trans*-splicing products detectable in the dRTM 31/1-FLAG and *COL7A1*-dTS-MG co-transfection experiments in HEK293. The *trans*-

splicing efficiency is decreased in the dRTM transfected dTS-MG-expressing cell line as shown in Figure 18a. Interestingly, other than in the GFP-based screening system (Figure 16) the dRTM 31/1-FLAG favoured the 3' *trans*-splicing over the 5 '*trans*-splicing reaction probably due to steric reasons (Figure 18a, b).

In Figure 18b an intensive gel band representing the 3' *trans*-splicing product and a comparatively weaker band representing 5' *trans*-splicing product are shown. GAPDH was used as a reference gene and loading control.

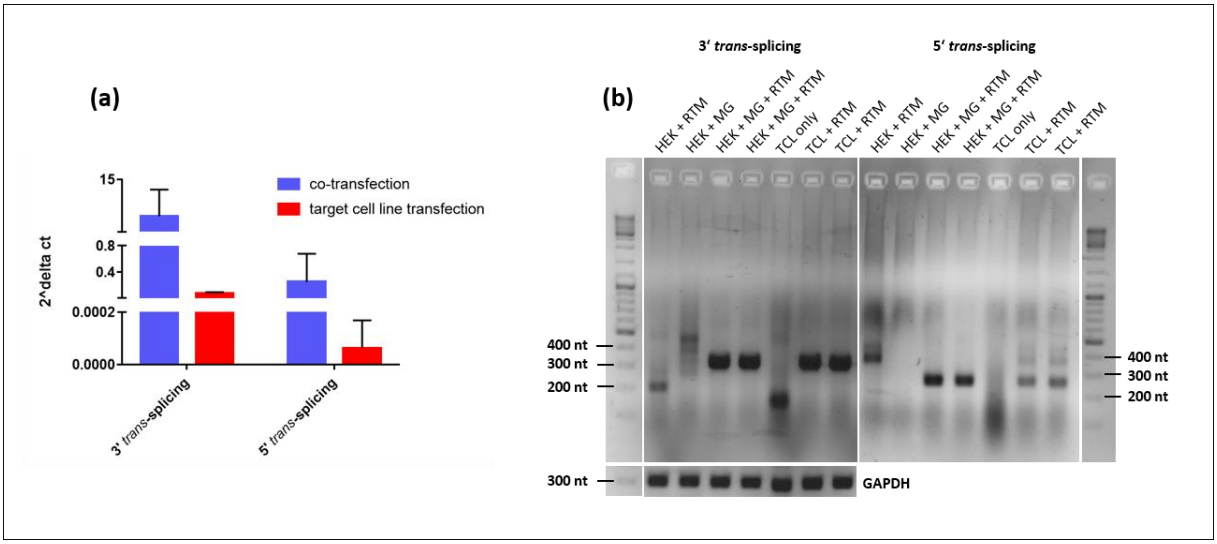

Figure 18. *Trans*-splicing efficiency of endogenous dRTM 31/1-FLAG in dTS-MG-expressing HEK293 cells. a) Using SqRT-PCR the levels of 3' and 5' *trans*-splicing events in, the co- (dRTM 31/1-FLAG (RTM) and *COL7A1*-dTS-MG (MG) into HEK293) and the single (dRTM 31/1-FLAG into HEK293 cells stably expressing the dTS-MG) transfection models were determined. These results confirmed those of the GFP-based screening system. The mean values + SD of three independent experiments are shown. **b)** The ratio between 3' and 5' *trans*-splicing shifted from 5' to 3' compared to the results achieved via the screening model (Figure 16). 3' *trans*-splicing products appeared at a size of 317 nt and were more intense than 5' product (227 nt) as can be seen in the agarose gel above. Especially regarding 5' *trans*-splicing the distinction between co-transfection (HEK + MG + RTM) and target cell line transfection (TCL + RTM) was visible.

3.3 Detection of endogenous double RNA *trans*-splicing

3.3.1 Double RNA *trans*-splicing in RDEB keratinocytes

To analyse the endogenous functionality the generated dRTM 31/1-FLAG was retrovirally transfected into RDEB patient keratinocytes. Therefore the dRTM was cloned into the retroviral vector pMX-*IRES*-Blasticidin. RNA was isolated from transfected RDEB cells and RT-PCR was performed to detect accurate double RNA *trans*-splicing.

A nested PCR on a PCR cloud representing the double *trans*-splicing product revealed the presence of 3' and 5' *trans*-splicing products separately indicating that the selected dRTM is able to induce both splicing reactions simultaneously. Initially, we performed PCR using a primer set binding exon 102 and exon 106. The double RNA *trans*-splicing product was 66 nt larger than the *cis*-splicing product (prominent band at a size of 267 nt), due to the 3x FLAG tag. The band at a size of 333 nt was extracted from the agarose gel and used as template for further nested PCRs to detect accurate 3' and 5' *trans*-splicing (Figure 19b). 3' (2) and 5' (3) *trans*-splicing products were detected and sequenced confirming the functionality of our generated dRTM 31/1-FLAG in RDEB patient keratinocytes (Figure 19c). The used primer pairs are displayed in Figure 19a.

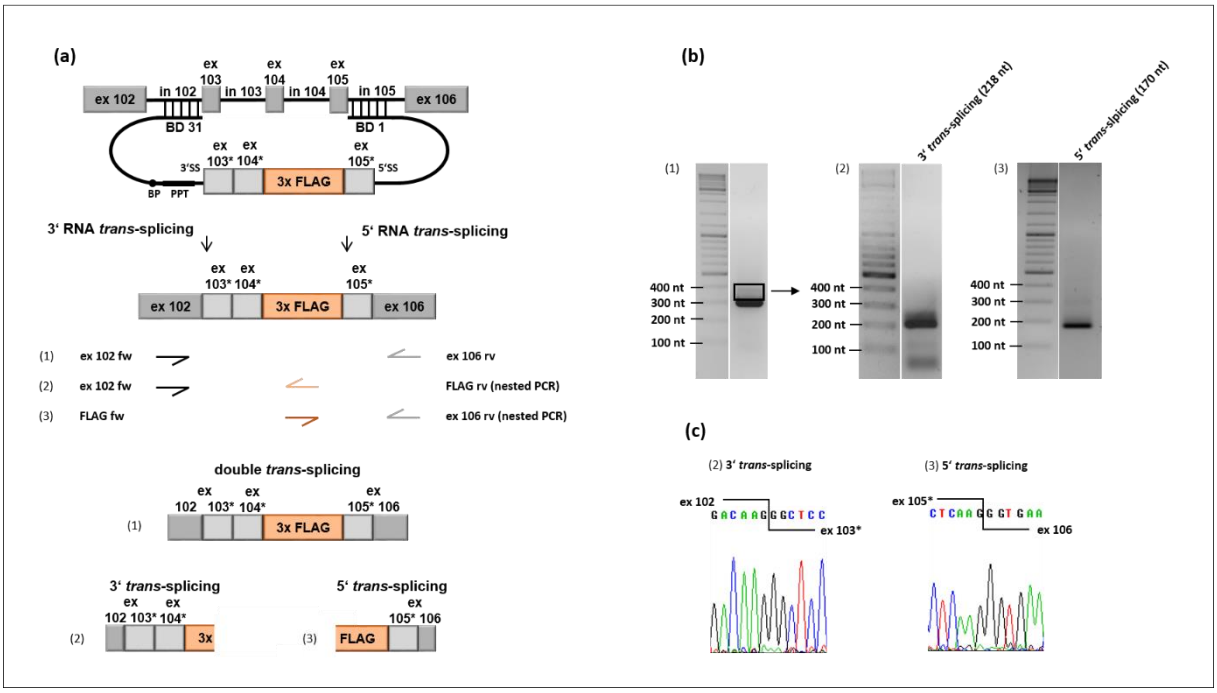

Figure 19. Analysis of endogenous double RNA *trans*-splicing in RDEB patient keratinocytes. a) Schematic description of the endogenous *trans*-splicing process induced by dRTM 31/1-FLAG. The dRTM contains silent mutations within the wild-type coding sequence of *COL7A1* spanning from exon 103 to exon 105 and a 3x FLAG tag for detection (modified exons are marked with a *). The applied primer sets for RT-PCR and the expecting double, 3' and 5' *trans*-splicing products are displayed. **b)** RNA from transfected RDEB keratinocytes was isolated and RT-PCR was performed for *trans*-splicing detection. Via nested PCR (template 333 nt of PCR (1)), it was possible to detect 3' *trans*-splicing (2) and the 5' *trans*-splicing product (3) at a size of 218 nt and 170 nt, respectively. **(c)** The accurate *trans*-splicing products were confirmed by sequence analysis.

3.3.2 Restoration of type VII collagen expression

Besides the retroviral vector system a lentiviral vector system was used in order to increase the transduction efficiency into patient keratinocytes. dRTM 31/1 was transduced into RDEB keratinocytes, containing an RDEB causing homozygous mutation in exon 105. Due to the fact that lentiviral vectors also transduce non-dividing cells the integration of dRTM 31/1 into the genome of RDEB keratinocytes should be facilitated. After transduction genomic DNA was isolated and the accurate integration was checked by PCR analysis using primer sets proving the presence of dRTM 31/1 in the genome (Figure 20).

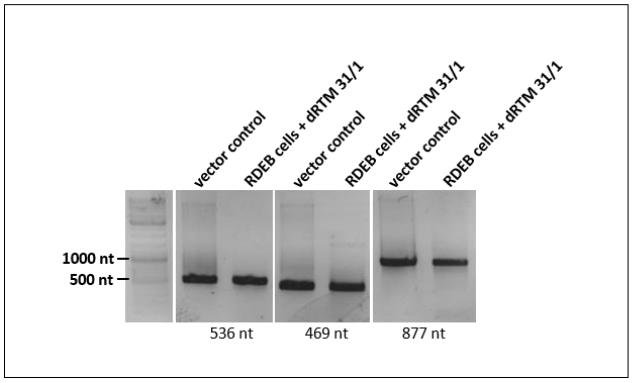

Figure 20. Integration check of dRTM 31/1 in RDEB keratinocytes. The proper genomic integration of dRTM 31/1 in RDEB keratinocytes after transduction was confirmed using specific PCRs. The integration of dRTM 31/1 in the genome of RDEB cells is shown. As vector control the lentiviral plasmid carrying dRTM 31/1 was included.

To analyse the restoration of type VII collagen expression via double RNA *trans*-splicing in RDEB keratinocytes, immunofluorescence microscopy was performed on human wild-type keratinocytes, patient keratinocytes and dRTM treated patient cells (Figure 21).

Figure 21a showed wildtype keratinocytes with proper type VII collagen expression, whereas untreated RDEB cells did hardly express type VII collagen (Figure 21b). dRTM transduced RDEB keratinocytes revealed type VII collagen correction and expression in individual patient cells as shown in Figure 21c. However, for further experiments single cell dilutions will be done to get a homogenous population with restored function of collagen type VII.

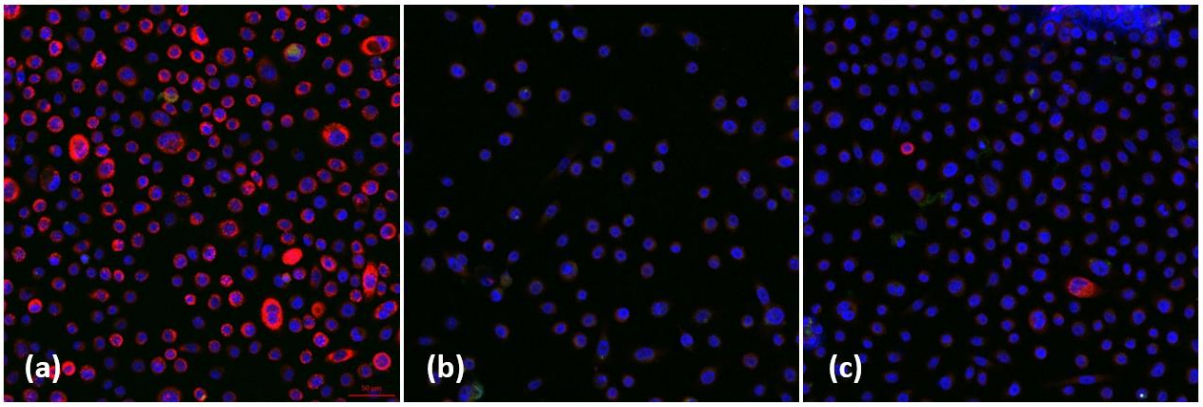

Figure 21. Immunofluorescence staining of transduced RDEB patient keratinocytes. (a) Wildtype keratinocytes showed an intense staining for type VII collagen (red) in the cytoplasm of the cells using a rabbit anti human polyclonal type VII collagen antibody. **(b)** RBED patient keratinocytes had a significantly decreased expression of type VII collagen and therefore act as negative control. Individual cells treated with dRTM 31/1 showed a restored expression of type VII collagen upon accurate double RNA *trans*-splicing **(c)**.

3.4 Antisense RNAs to enhance *trans*-splicing efficiency

Recent studies have shown that antisense RNAs can increase the *trans*-splicing efficiency of a given RTM via blocking of competitive *cis*-splice sites within the target pre-mRNA region [57,70,72]. Koller *et al*. (2015) selected a randomly designed antisense RNA (asRNA 13) binding *cis*-splicing elements within the intron 102/exon 103 junctions and exon 103 of *COL7A1*, respectively. Thus increased the *trans*-splicing efficiency via 3' *trans*-splicing up to 12 fold [70]. Due to these promising results we aimed to increase the double RNA *trans*-splicing efficiency of dRTM 31/1 via rationally designed antisense RNAs binding to distinct areas of our generated *COL7A1*-dTS-MG as displayed in Figure 22b. All individual asRNAs, generated via PCR amplification and subsequent cloning into a pcDNA 4.0 expression vector, were co-transfected with the screening dRTM 31/1-int. acGFP and *COL7A1*-dTS-MG into HEK293 cells. The *trans*-splicing efficiency was evaluated by flow cytometric analysis of treated cells. As shown in Figure 22a most tested asRNAs were able to enhance the double RNA *trans*-splicing efficiency in comparison to cells, in which the empty (without asRNA) pcDNA 4.0 expression plasmids (negative control) were transfected together with the screening plasmids. The most promising asRNAs asRNA 6, asRNA 8 and asRNA 9, induced a 10-12 fold increase in the amount of GFP-expressing cells compared to the negative control three days post treatment. The binding sites of the selected asRNAs are shown in Figure 22b. Additionally, the functionality of the selected asRNAs were verified via SqRT-PCR (Figure 22c, d) confirming their potential to increase the efficiency of 3' and 5' *trans*-splicing, respectively.

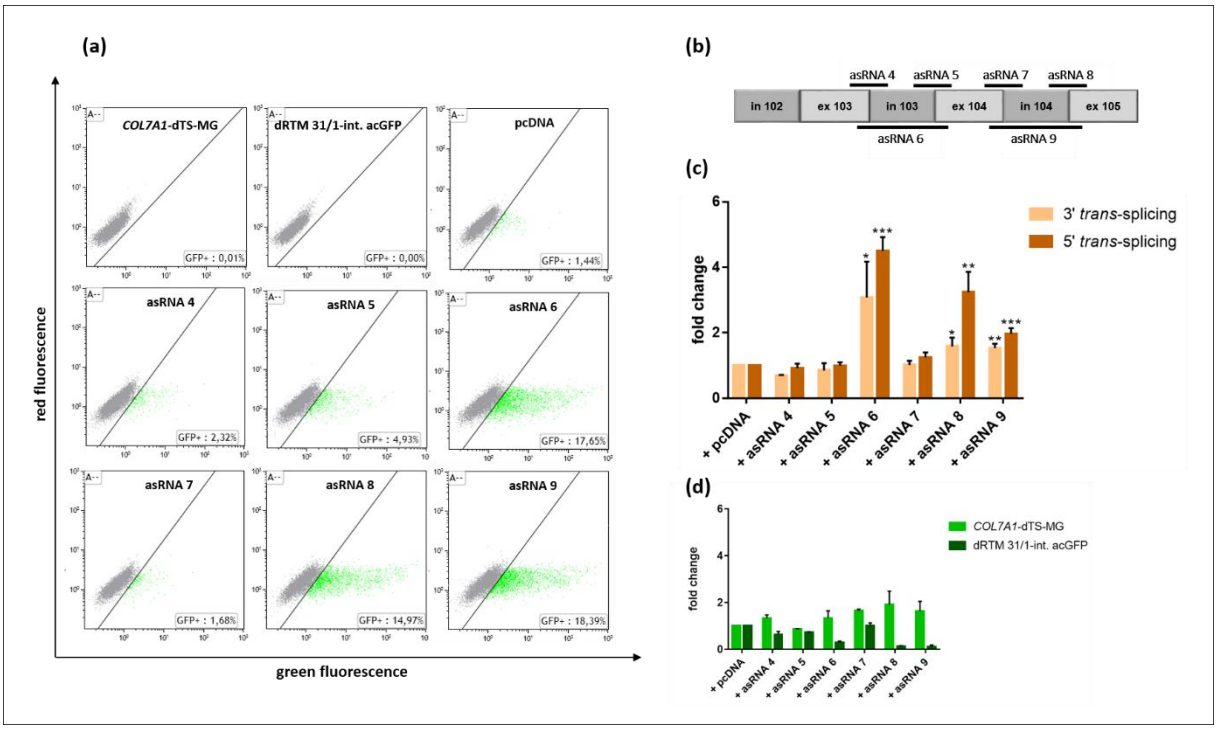

Figure 22. Inclusion of antisense RNAs to increase *trans*-splicing efficiency induced by dRTM 31/1. (a) First of all, rational designed antisense RNAs (asRNAs) were screened for their ability to enhance the *trans*-splicing efficiency between the *COL7A1*-dTS-MG and dRTM 31/1-int. acGFP in HEK293 cells. Therefore, flow cytometric analysis was performed to identify the most promising asRNA candidates. asRNA 6, asRNA 8 and asRNA 9 were able increase the double *trans*-splicing levels 10-12 fold. HEK293 cells, transfected with dRTM, MG and empty pcDNA 4.0 lacking of asRNA sequences served as negative control and reference. **(b)** Here the schematic representation of the asRNA binding sites within the dTS-MG is shown. **(c)** To quantify the level of accurate RNA *trans*-splicing on RNA level SqRT-PCR was performed to specifically detect 3' and 5' *trans*-splicing products separately confirming the results achieved by flow cytometric analysis. The mean values + SD of three different experiments are shown. An unpaired, two-tailed *t*-test was performed with GraphPad Prism 7 software (San Diego, CA, USA) to prove the statistical significance between asRNA 6 (* *p* value = 0,0301; *** *p* value = 0,0001), asRNA 8 (* *p* value = 0,0207; ** *p* value = 0,0033) and asRNA 9 (** *p* value = 0,0026; *** *p* value = 0,0007) and the control pcDNA. **(d)** To assign the impact of the asRNAs on *trans*-splicing increase, the expression of *COL7A1*-dTS-MG and dRTM 31/1-int. acGFP were measured additionally. The expression level of both molecules was similar in all samples. The mean values + SD of three different experiments are shown.

Using primers, which bind the junction of 5' acGFP/internal acGFP and internal acGFP/3' acGFP, it was possible to quantify the double RNA *trans*-splicing levels. The dTS efficiency was significantly increased by the presence of asRNA 9 (Figure 23).

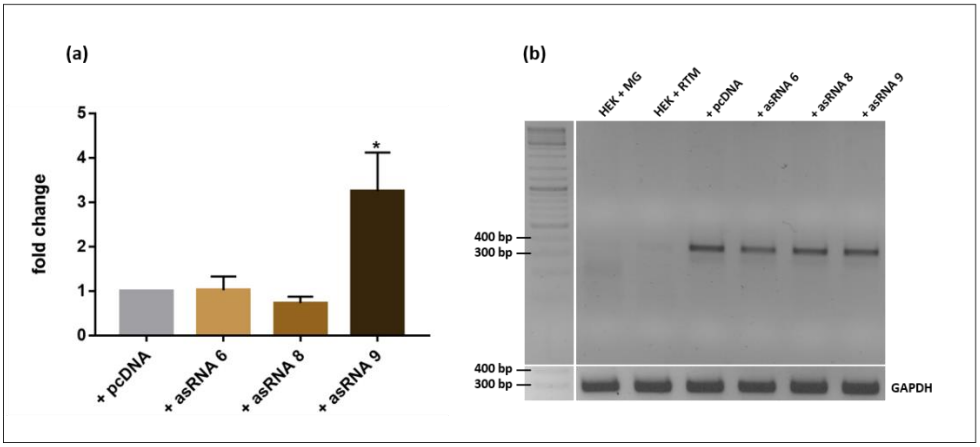

Figure 23. Quantification of full-length GFP after dTS-MG, dRTM, asRNA treatment of HEK293 cells. (a) To quantify double RNA trans-splicing levels after the introduction of the screening molecules together with individual asRNAs into HEK293 cells. SqRT-PCRs were performed using 5' acGFP/internal acGFP and internal acGFP/3' acGFP specific primer pairs. If double RNA trans-splicing occurred, full-length GFP was generated and expressed. asRNA 9 seemed to have the most impact on the efficiency of double RNA trans-splicing evaluated in the screening model. The mean values + SD of three different experiments are shown. An unpaired t-test (two-tailed) using GraphPad Prism 7 software (San Diego, CA, USA) confirmed the statistical significant increase in asRNA 9 compared to the control pcDNA (* p value = 0,0112). (b) The PCR product with a size of 345 nt was visible on the gel; housekeeping gene (GAPDH) expression was nearly the same in all different samples. The transfection of either COL7A1-dTS-MG (MG) or dRTM 31/1-int. acGFP (RTM) in HEK293 served as the negative controls. For measuring the enhancement of trans-splicing efficiency concerned by asRNAs, HEK293 cells were transfected either with RTM, MG and pcDNA 4.0 as the reference, or with RTM, MG and one of the promising asRNA candidates.

4 Discussion

Spliceosome mediated *trans*-splicing is an elegant method to convert genetic disease-causing mutations into wild-type sequences of a gene on mRNA level. By combining 3' and 5' *trans*-splicing for gene repair, it is possible to exchange single or internal affected exons of a certain gene.

In general, the efficiency of RNA *trans*-splicing is low, thus the design of dRTMs is of main importance. So far there are only a few publications available, in which major aspects and guidelines for RTM design are discussed [67,74]. In general the focus lays on optimization of binding, splicing and coding domains. Additionally Philippi *et al*. (2015) also showed the importance of 3' splice sites strength of the target intron, upstream to the to be exchanged exon, in respect of 3' *trans*-splicing efficiency [55]. Also the deletion of competitive cryptic splice sites, to decrease competing splicing reactions, can increase the *trans*-splicing efficiency [74,75].

However, Murauer *et al.* (2011) recently demonstrated, that the *trans*-splicing efficiency of a designed RTM can be sufficient to correct an RDEB phenotype *in vitro* using a 3' *trans*-splicing strategy [43]. Additionally, Peking *et al.* (2016) showed the possibility to reprogram murine *Col7a1* via 5' *trans*-splicing [45]. Philippi *et al*. (2015) showed the repair of dysferlin and the right localization of the restored protein within the skeletal muscle *in vivo* [55]. Although these *trans*-splicing strategies are promising for future investigations in a pre-clinical setting we thought about ways to repair mutations within *COL7A1* localized within internal parts of the gene. By combination of 5' and 3' *trans*-splicing it should be possible to exchange internal exons in an affected gene on RNA level thereby reducing the size of the RTM significantly.

In this master thesis we investigated the double RNA *trans*-splicing induced RNA repair of a homozygous mutation within exon 105 of *COL7A1*, leading to the dystrophic form of epidermolysis bullosa. After selection of optimal dRTM binding regions within intron 102 and 105 of *COL7A1* using our fluorescence-based screening system, respectively, we designed a highly functional dRTM capable to exchange exon 103 to the affected exon 105 with the wild-type *COL7A1* sequence provided by the dRTM. The double *trans*-splicing molecule 31/1 was already constructed and provided for the experiments. BD 31 (109 nt) binds intron 102 and BD 1 (122

nt) intron 105; these two binding domains were selected due to their promising *trans*-splicing efficiencies evaluated via the RTM screening model before.

Prior to testing the endogenous functionality of our selected dRTM in RDEB patient keratinocytes, the *trans*-splicing efficiency of dRTM 31/1 was validated using in the fluorescence-based screening setting. For that the dRTM 31/1, carrying the internal part of acGFP instead of the wild-type sequence of *COL7A1*, was investigated in co-transfection experiments together with the *COL7A1*-dTS-MG in HEK293 cells or in single transfection experiments in HEK293 cells stably expressing the *COL7A1*-dTS-MG. Flow cytometric analysis of treated cells revealed the restoration of GFP expression via double RNA *trans*-splicing in about 15 % of co-transfected HEK293 cells. In contrast to that, in stably-*COL7A1*-dTS-MG expressed cell line only 1 % of all analysed cells expressed GFP probably due to the weak expression of the MG. Due to the random integration of one or more copies of the MG into the genome via the Piggy Bac transposon system the expression level is expected to be different from cell to cell. Additionally, recent studies showed that the efficiency of *trans*-splicing is higher, if both interaction partners (target pre-mRNA and RTM), are expressed extra-chromosomally. Reason for that is the local proximity of both molecules, present in huge amounts, and therefore the higher chance to interact with each other [76,77]. Nevertheless the stable MG expression setting is more comparable with the endogenous situation within RDEB patient cells. SqRT-PCR experiment on the RNA of treated cells confirmed the results achieved by flow cytometric analysis. The levels of 3', 5' and double *trans*-splicing are higher in the co-transfection system in comparison to the single transfection system. Although the two separate *trans*-splicing reactions (3' and 5') did not reveal the same level of *trans*-splicing efficiency in both systems, full-length GFP was restored in high levels semi-quantified by SqRT-PCR and additionally shown in protein level by flow cytometric analysis. In general in the screening setting the 5' *trans*-splicing was favoured against the 3' *trans*-splicing reaction. The challenge of double RNA *trans*-splicing is standing out here, because in theory a dRTM should be designed with two equally efficient binding domains. However this is very difficult as the efficacy of *trans*-splicing is not defined only by the binding position of RTM at the target region but also by other endogenous splicing signals like ESEs and ESSs, the strength of 3' SS in target introns and the design of splicing and coding domains [52,55].

Prior to the endogenous setting in RDEB keratinocytes, the internal acGFP part of dRTM 31/1 was replaced with the coding domain (exon 103 to exon 105 of *COL7A1*), either containing or lacking a 3x FLAG tag in between exon 104 and exon 105. Additionally, cryptic *cis*-splice sites within the dRTM were deleted by the inclusion of silent mutations to minimise undesirable *cis*- and *trans*-splicing events. We have shown that dRTM 31/1 induced double RNA *trans*-splicing in the MG-expressing cell line. The 3' and 5' *trans*-splicing products were verified by sequence analysis. Similar to the disparities in *trans*-splicing events in the co-transfection and the target cell line transfection in the screening model, the efficacy of *trans*-splicing induced by the endogenous dRTM 31/1-FLAG in the *COL7A1*-dTS-MG stably expressing target cell line was decreased. In both models 3' *trans*-splicing was preferred, which is contrary to results achieved with the screening dRTM containing the internal acGFP part. We suggested that somehow the conformation of the internal acGFP part, carried by the screening dRTM, has a sterical influence on the interaction of the target pre-mRNA with the dRTM different to the endogenous dRTM lacking the reporter sequence. This phenomenon showed that the preference for one splicing reaction (3' or 5') in a double RNA *trans*-splicing context is dependent on the conformation of both molecules during the splicing reaction(s), the size of the dRTM sequence to exchange or in general the strength of both splice sites.

In order to analyse the endogenous *trans*-splicing efficiency of our generated dRTM we transiently introduced it into patient keratinocytes carrying a homozygous mutation within exon 105. Nested RT-PCRs on a primary PCR product representing the expected double RNA *trans*-splicing product confirmed accurate 3' and 5' *trans*-splicing products, thus indicating the capability of our selected dRTM to exchange internal *COL7A1* exons. Due to the fact that the *trans*-splicing efficiency in the endogenous situation is expected to be decreased compared to that detected via our fluorescence-based screening system due to the weaker target pre-mRNA expression, it is comprehensible that a nested PCR is needed for detection.

Additionally, the stable integration of the endogenous dRTM 31/1 into the genome of patient cells enables the analysis of collagen type VII restoration upon accurate double RNA *trans*-splicing. The presence of restored type VII collagen in RDEB keratinocytes as a consequence of double RNA *trans*-splicing induced by dRTM 31/1 was shown by immunofluorescence staining using anti *COL7A1* antibody in individual cells. However, due to the obvious low *trans*-splicing we were not able so far to detect accurate double RNA *trans*-splicing on mRNA level.

Therefore single cell dilutions will be performed in order to facilitate the analysis of *COL7A1* repair in future experiments on RNA and protein level.

The second aim in this study was the inclusion of antisense RNAs, blocking competitive target pre-mRNA splice sites, in order to further increase the *trans*-splicing efficiency of our selected dRTM 31/1. Therefore we have utilized our fluorescence-based screening system to accelerate and facilitate the selection of promising asRNAs. Up to date several groups are dealing with this topic [57,70–72]. In our study antisense RNAs were designed specific for one or two target *cis*-splice sites located within the target pre-mRNA region spanning from exon 103 to exon 105. asRNA 4, 5, 7 and 8 have a size of 30-40 nt and asRNA 6 and 9 a size of about 300 nt. Flow cytometric analysis and SqRT-PCR on RNA of dRTM, MG and asRNA transfected HEK293 cells revealed asRNA 6, 8 and 9, inducing GFP-expression in about 14-19 % of all analysed cells (reference pcDNA: 1,4 % GFP positive cells), as most auspicious asRNA members to enhance 3' and 5' *trans*-splicing. asRNA 9 showed the best ability to enhance the level of double RNA *trans*-splicing manifesting in a 3-4 fold expression of full-length GFP. Noticeably, all three selected asRNAs were specific for the internal target *cis*-splice sites within the *COL7A1*-dTS-MG.

In conclusion, we could detect double RNA *trans*-splicing both in the screening model and in the endogenous system in HEK293 cells and RDEB patient keratinocytes. We could detect restored type VII collagen in lentiviral treated RDEB keratinocytes. Additionally, using our screening system we were able to select asRNA capable to further enhance the *trans*-splicing efficiency of dRTM 31/1. The efficacy of double RNA *trans*-splicing turned out to be very low and incredibly tough to detect. Therefore single clonal cell isolation after dRTM treatment is crucial for further investigations, including the detection of accurate double RNA *trans*-splicing product via sqRT-PCR on RNA level and via western blot analysis on protein level.
Finally, double RNA *trans*-splicing is a promising tool to reverse individual genetic mutations within the middle of a gene by exchanging the affected exons against the wild-type sequence of this gene. The fluorescence-based screening system, established in the lab, is an auspicious technology to identify efficient and specific RNA *trans*-splicing molecule prior to subsequent experiments in DEB patient keratinocytes.

5 Materials and Methods

5.1 Cell lines

5.1.1 HEK293

All screening experiments and co-transfections were done in the human embryonic kidney cells line HEK293 AD (Stratagene, La Jolla, CA, USA) and in HEK293 cells, which stably-expressing a *COL7A1*-double *trans*-splicing-minigene. HEK293 FT cell line (Invitrogen, Carlsbad, CA; [78]) was used for the production of lentiviral particles. These cell lines were grown in Dulbecco DMEM FG0445 (Biochrom, Berlin, GER) supplemented with 10 % FCS and 100 U/ml penicillin/100 µg/ml streptomycin (Biochrom, Berlin, GER) in an incubator at 37°C with 5 % CO_2 and passaged every 4-5 days.

5.1.2 RDEB patient cells

For endogenous studies immortalized RDEB patient keratinocytes carrying a homozygous mutation in exon 105 (R2610X) were cultivated in SFM medium (Life technologies, Carlsbad, CA, USA) supplemented with the included additions (2,5 µg EGF Human Recombinant; 25 mg Bovine Pituirary Extract) and 100 U/ml penicillin/100 µg/ml streptomycin (Biochrom, Berlin, GER) at 37°C and 5 % CO_2 in the incubator. For proof of principle experiments RDEB keratinocytes were used and cultivated at same conditions. The RDEB keratinocytes line derived from a patient harbouring a homozygous mutation in exon 105 (R2610X) was kindly provided by Prof. Guerrino Meneguzzi, Nice, France. Because of their robustness, they turned out to be a good model for the examination of *trans*-splicing. These cell lines were passaged 3 times a week.

5.2 The fluorescence-based screening system

5.2.1 Overview about the screening system and constructs

The screening dRTM 31/1 contains the internal part of the green fluorescence protein (int. acGFP) flanked by two BDs BD31 and BD1. The sequence of BD 31 (5'-GCCCCTTCATGGGGCCAA TCCACGGAACTCTCCTAACCTCACACCAAAACCTTGGGCCCTCCCTGGGGCCCCTCCTCTCGGCCACT CCATAATCAACCACAAAACCCCT-3') is complementary to 109 nt of intron 102 of *COL7A1*. The binding domain for 5' *trans*-splicing induction, BD 1 (5'-TCAACTACTCCAACCTCTGACCCAATGCC CTAATATCTGACCCCAAATCCCTCGCCCTTCAACATTGGGCCTTCCTGACCGGAAAAAAACCAATCTT GCTTCTTTCCTACCTTGGGGCCCCG-3'), binds to 122 nt of the junction between exon and intron 105. The screening dRTM was generated according to previously published protocols [52,67,69,69,70] and was kindly provided by Dr. Ulrich Koller. To analyse the *trans*-splicing efficiency the screening dRTM was transfected either together with a provided *COL7A1*-double *trans*-splicing-minigene (*COL7A1*-dTS-MG) into HEK293 cells (Stratagene) or in a target HEK293 cell line, stably expressing the *COL7A1*-dTS-MG, respectively [70]. The *COL7A1*-dTS-MG consists of the 3' acGFP part, the 5' acGFP part and in between the type VII collagen coding sequence spanning from intron 102 to intron 105 [67,69,70]. Accurate double RNA *trans*-splicing between the dRTM and the MG leads to the fusion of all three GFP parts, provided by both interaction partners, manifested in the expression of full-length GFP [52] (Figure 24).

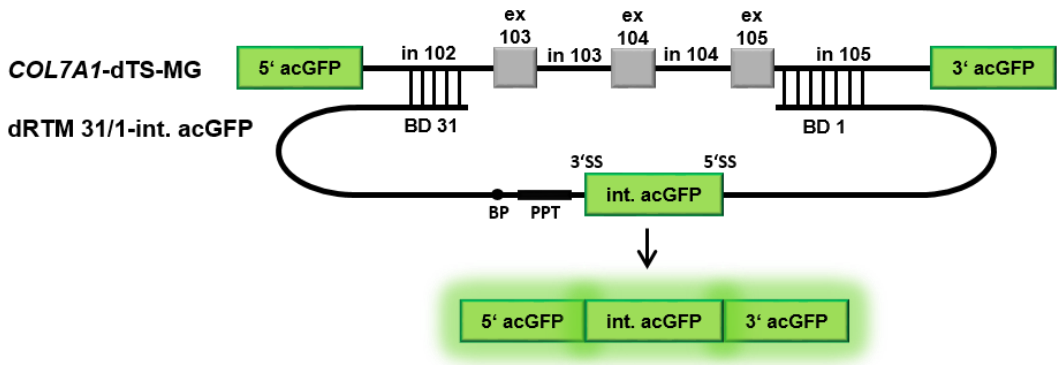

Figure 24. Depiction of double RNA-*trans* splicing using the fluorescence-based screening system. The *COL7A1*-double *trans*-splicing-minigene (*COL7A1*-dTS-MG) carries the 5' and 3' portion of a green fluorescence protein (acGFP) and the *COL7A1* sequence spanning from intron 102 to intron 105. The screening double RNA-*trans*-splicing molecule (dRTM) 31/1 contains two binding domains BD 31 and BD 1, splicing domains and the internal part of acGFP. If *trans*-splicing occurs, detectable full-length GFP is generated.

To enhance the double *trans*-splicing efficiency induced by the screening dRTM 31/1, antisense RNAs were included in the transfection of HEK293 cells.

5.2.2 Cloning of antisense RNAs

One aim of these studies was the generation of antisense RNAs (asRNA), which bind *cis*-splice sites to increase the *trans*-splicing efficacy induced by dRTM 31/1. Different asRNAs binding different intron and exon regions were rationally designed and amplified by PCR using genomic DNA of wild-type human keratinocytes as template. Primers established for this approach carried an EcoRI and a BamHI restriction site. Applied primers are listed below: asRNA 4 (exon/intron 103 forward 5'-GATCGAATTCACCCCAGGCAAGTTCTGCCC-3'; intron 103 reverse 5'-GATCGGATCCACCTGGGCCTGGGCCTG-3'), asRNA 5 (intron 103 forward 5'-GATCGAATTCGAAGGGCTCCCCCATCTG-3'; intron 103/exon 104 reverse 5'-GATCGGATCCCCAGGTTGACCCTGTGAGAAA-3'), asRNA 6 (exon/intron 103 forward 5'-GATCGAATTCCCCCAGGCAAGTTCTGCCC -3'; intron 103/exon 104 revers 5'-GATCGGATCCTTGACCCTGTGAGAAACACAGAT-3'); asRNA 7 (exon/intron 104 forward 5'-GATCGAATTCGACCCGGTAAGATGCCCCT-3'; intron 104 reverse 5'-GATCGGATCCCCCCTGTGGGAGCAGGG-3'), asRNA 8 (intron 104 forward 5'-GATCGAATTCTCCTCTGACCTCACATGGAC-3'; intron 104/exon 105 reverse 5'-GATCGGATCCGGGATCCCTAGCAGGGAG-3') and asRNA 9 (exon/intron 104 forward 5'-GATCGAATTCGACCCGGTAAGATGCCCCT-3'; intron 104/exon 105 reverse 5'-GATCGGATCCGGATCCCTAGCAGGGAGA-3'). Agarose gel electrophoresis (2 % agarose gel) verified the correct size of the different antisense asRNAs (asRNA 4 - 36 nt, asRNA 5 - 41 nt, asRNA 6 - 261 nt, asRNA 7 - 32 nt, asRNA 8 - 42 nt, asRNA 9 - 340 nt), the bands were excised from the gel and purified using the illustra™ GFX™ PCR DNA and Gel Band Purification Kit (GE Healthcare, Little Chalfont, UK). The different asRNAs were separately cloned into pcDNA 4.0 (Invitrogen, Carlsbad, CA, USA) by restriction using BamHI and EcoRI (FastDigest Enzymes of Thermo Fisher Scientific, Waltham, MA, USA). The sequences of the antisense RNAs and the correct position in pcDNA 4.0 were approved by sequence analysis. As an example, asRNA 6 in pcDNA 4.0 is shown in the vector map below in Figure 25.

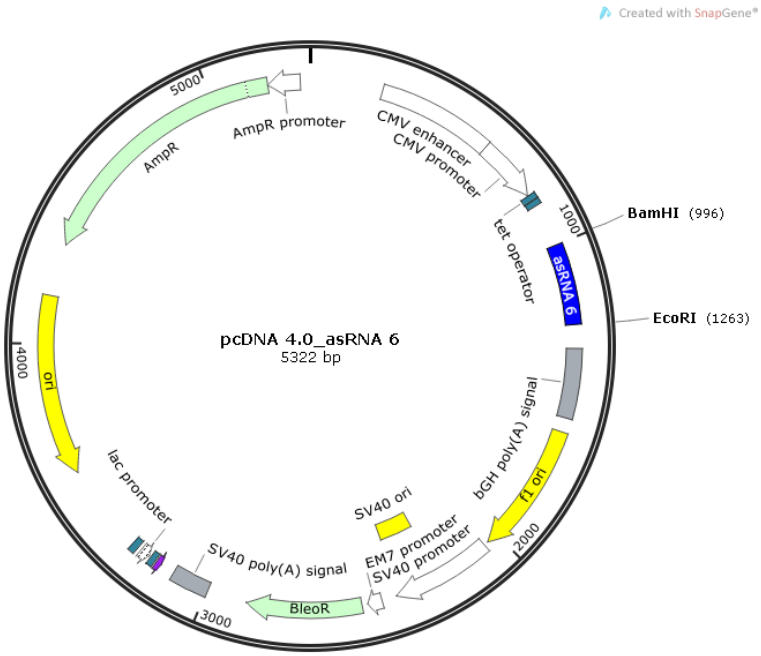

Figure 25. pcDNA 4.0 with asRNA 6 cloned in it. asRNA 6 is shown in dark blue. BamHI and EcoRI restriction sites are plotted in the plasmid map. The plasmid card was created using SnapGene® Viewer 2.3.3.

5.2.3 Sequencing analysis

Sequencing of putative positive plasmids was done by using the BigDye Terminator sequencing kit (Applied Biosystems, Forster City, CA, USA). For this second generation sequencing ≥100 ng/µl plasmid DNA, Sequencing premix, 5x Sequencing buffer and forward or reverse primer [100 µM] were put together and a sequencing PCR was affiliated. The program began with 96°C for 1 min, 30 cycles of 96°C for 10 seconds, 50°C for 5 seconds and 60°C for 90 seconds, and ended with 4°C for infinite time. This probes were sent to the in-house sequencer and were analysed using Chromas 1.56 from Technelysium Pty Ltd (South Brisbane, AUS).

5.2.4 Transient transfection of screening molecules in HEK293 cells

For transient transfection of HEK293 cells and *COL7A1*-dTS-MG stably-expressing HEK293 cell line with the screening constructs jetPEI reagent (Polyplus-tranfection SA, Illkirch, France) was used. Usually 1-6 µg of DNA were transfected into cells according to the manufacturer's protocol in 60 mm plates.

5.2.5 Flow cytometric analysis

dRTM and *COL7A1*-MG co-transfected HEK293 cells and single RTM transfected HEK293 cell line, stably-expressing the MG, were evaluated by flow cytometric analysis according to their GFP expression. Two or three days post transfection the cells were washed in Phosphate Buffered Saline PBS (Sigma-Aldrich, St. Louis, MO, USA), trypsinized (1-2 ml trypsin (0,05%) - EDTA (0,02%) (Biochrom, Berlin, GER) in solution A) and centrifuged at 350 g for 5 minutes at room temperature. Afterwards supernatant was discarded and the cell pellet was resuspended in about 500 µl PBS. The analysis of GFP expression occurred in the Beckman Coulter FC-500 FACS analyser (Beckman Coulter, Vienna, AUT) and the data were evaluated with Kaluza 1.3 software (Beckman Coulter, Brea, CA, USA).

5.2.6 RNA isolation

For Isolation of RNA from cells 2-3 days post transfection RNeasy® Mini Kit (QIAGEN, Venlo, NLD) was used according to the manufacture's protocol. Cells were harvested by centrifugation at 350 g for 5 minutes in a 1,5 ml tube and thereafter resuspended and lysed in 350 µl RLT buffer containing 1 % β–mercaptoethanol (Sigma-Aldrich, St. Louis, MO, USA). After incubation the lysates were homogenized through a needle, one volume 70 % EtOH was added and the mixture was transferred to the RNeasy column. After certain centrifugation and washing steps, the RNA was eluted in 35-50 µl RNAse free water and stored at -20°C and for long-time storage at -80°C.

5.2.7 Determination of *trans*-splicing efficiency in screening systems by SqRT-PCR

Semi quantitative real time PCR (SqRT-PCR) was performed using the CFX96 Real Time System C1000 Thermal Cycler (Bio-Rad Laboratories GmbH, Munich, DE) to quantify 3', 5' and double *trans*-splicing levels in dRTM 31/1-int. acGFP and *COL7A1*-dTS-MG treated HEK293 cells and MG stably-expressing HEK293 cells. RNA was isolated 2-3 days post transfection and analysed via GoTaq® 1-Step RT-qPCR.

The PCR reactions contained 10 µl SYBR Green Mix (Promega, Madison, WI, USA), 0,4 µl 1-Step-RT (Promega, Madison, WI, USA), 0,6 µl primer mix (forward and reverse primer, 10 µM

each) and 1 µl RNA template (100 - 500 ng). Cycling conditions for detection of *trans*-splicing efficiency were: 15 min at 37°C (reverse transcription), 10 min at 95°C (RT inactivation/hot-start activation), 50 cycles of 10 sec at 95°C (denaturation), 20 sec at 60/72°C (annealing) and 20 sec at 72°C (extension). An additional melting curve analysis was attached to the SqRT-PCR protocol (95°C for 10 sec, 65-95°C in 0,5°C increments for 5 sec) to test the specificity of the resulting PCR product.

PCR products were analysed on a 2 % agarose gel and verified by sequence analysis. Each run was repeated at least three times, the samples were measured in duplicates and the *trans*-splicing levels were calculated after normalization to the house keeping gene GAPDH. For detection of *trans*-splicing in the screening system for 3' *trans*-splicing 5' acGFP primer (forward: 5'-GGGCGCCGAGCTGTTCACCGGCA-3') and internal acGFP primer (reverse: 5'-GGTATCGCCCTCGAACTTCAC-3'), for 5' *trans*-splicing an internal acGFP primer (forward: 5'-GGCGTGCAGTGCTTCTCACGCTACCCCG-3') and a 3' acGFP primer (reverse: 5'-CGCCGATGGGGGTATTCTGCTGG-3') were used. To detect the double RNA *trans*-splicing primers binding the junction of 5' acGFP and internal acGFP (forward: 5'-GTGCCCTGGCCCACCCTGGTGAC-3') and the fusion of int. acGFP and 5' acGFP (reverse: 5'-GTGGCGGATCTTGAAGTTCACCTTG-3') were used. For 5' and 3' *trans*-splicing confirmation a primer annealing temperature of 60°C and for the detection of accurate double *trans*-splicing 72°C were selected.

To detect the influence of antisense RNAs (asRNA 4-9) identical SqRT-PCR conditions and primers were used as mentioned above.

5.3 Functionality tests of dRTM in HEK293 cells

5.3.1 Overview about the system and constructs

Prior to endogenous experiments in patient keratinocytes, we tested the dRTM in HEK293 cells and in *COL7A1* stably-expressing HEK293 cells. For that the internal acGFP part of the screening dRTM was exchanged by modified exon 103 to 105 of *COL7A1* (cryptic *cis*-splice site removed by inclusion of silent mutations) and in between a 3x FLAG tag (Figure 26). This dRTM 31/1-FLAG was kindly provided from Dr. Ulrich Koller.

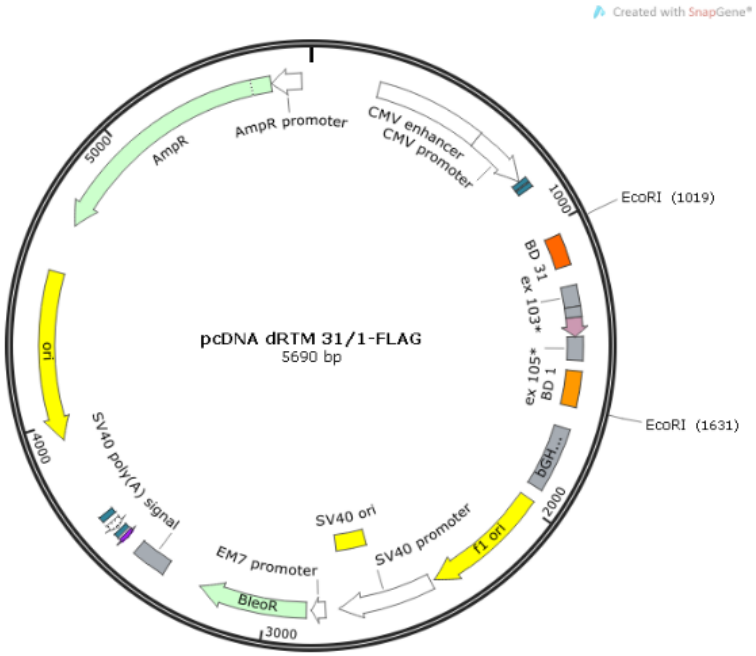

Figure 26. pcDNA vector containing dRTM 31/1-FLAG. In light and dark orange the binding domains BD 31 and BD 1 are visible. Modified exon 103*, exon 104* and exon 105* are shown in grey and the pink arrow should demonstrate the 3x FLAG tag. Plasmid map was generated using SnapGene® Viewer 2.3.3.

In these experiments the *COL7A1*-dTS-MG, mentioned in the upper section, was also used. To analyse accurate *trans*-splicing, the 3x FLAG tag containing dRTM was transfected either together with the provided *COL7A1*-dTS-MG into HEK293 cells or in a target HEK293 cell line, which stably-expressing the *COL7A1*-dTS-MG, respectively. If double RNA *trans*-splicing occurs, a product is generated consisting of 5' and 3' acGFP of the *COL7A1*-MG and modified exon 103 to 105 plus FLAG tag of the dRTM (Figure 27).

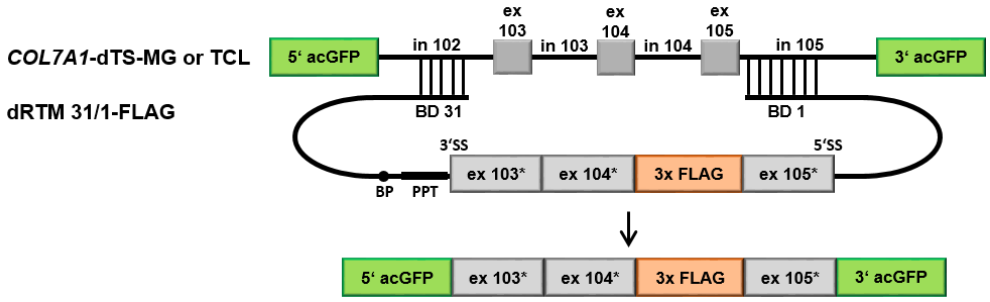

Figure 27. Schema of double *trans*-splicing induced by dRTM 31/1-FLAG. After co-transfection of dRTM 31/1-FLAG and *COL7A1*-dTS-MG in HEK293 cells or single transfection of dRTM 31/1-FLAG into HEK293 cells, stably-expressing the *COL7A1*-MG, the 5’ and 3’ ends of GFP are fused with the coding sequence provided by the dRTM via double RNA *trans*-splicing.

The transient transfection was performed as described in 5.2.4.

5.3.2 cDNA synthesis

RNA was isolated as mentioned in 5.2.6.

To get rid of genomic DNA contaminations 2 µg of the isolated RNA were treated with DNase I using DNase I Kit, Amplification Grade (Sigma Aldrich, St. Louis, MO, USA) at room temperature. The reaction was stopped after 20-30 min by DNase Stop-Solution and incubating the mixture at 70°C for 10 minutes.

To convert DNase I digested RNA into DNA, a cDNA synthesis was performed utilizing i-Script cDNA Synthesis Kit (Bio-Rad, Hercules, CA, USA). cDNA synthesis occurred at following conditions: 25°C for 5 min, 42°C for 30 min, 85°C for 5 min.

5.3.3 *Trans*-splicing detection by reverse transcriptase PCR

To verify the potential of dRTM 31/1-FLAG to induce double RNA *trans*-splicing in HEK293 cells stably-expressing the *COL7A1*-MG, total RNA of transfected cells was isolated and cDNA was synthesised. Reverse transcriptase PCRs (RT-PCR) were performed using the GoTaq DNA polymerase (Promega, Madison, MI, USA). For detection of 3’ *trans*-splicing a FLAG binding forward primer (5’-CTACAAAGACCATGACGGTGATTATAAAGATCATG-3’) and a 3’ acGFP binding reverse primer (5’-CGCCGATGGGGGTATTCTGCTGG-3’) were used. 5’ *trans*-splicing were determined by using a 5’ acGFP primer (forward 5’- GGGCGCCGAGCTGTTCACCGGCA-3’) and a FLAG tag reverse primer (5’-CATGATCTTTATAATCACCGTCATGGTCTTTGTAG-3‘). The RT-PCR products were detected via agarose gel electrophoresis, purified and verified by sequence analysis (5.2.3).

5.3.4 SqRT-PCR for determination of dTS efficiency induced by dRTM 31/1-FLAG

SqRT-PCR was performed as described in 5.2.7. To investigate 3' and 5' *trans*-splicing induced by endogenous dRTM 31/1-FLAG in HEK293 cells (co-transfection together with *COL7A1*-dTS-MG) and in stably-expressing *COL7A1*-MG HEK293 cells, SqRT-PCRs using GoTaq® 1-Step RT were performed. For PCR amplification of 3' *trans*-splicing products a 5' acGFP specific forward primer (5'-GGGCGCCGAGCTGTTCACCGGCA-3') and a 3x FLAG tag specific reverse primer (5'-CA TGATCTTTATAATCACCGTCATGGTCTTTGTAG-3') were used. For the verification of 5' *trans*-splicing a 3x FLAG tag binding forward primer (5'-CTAC-AAAGACCATGACGGTGATTATAAAGATC ATG-3') and a 3' acGFP specific reverse primer (5'-CGC-CGATGGGGGTATTCTGCTGG-3') were included. The PCR products were detected on an agarose gel and verified by sequencing analysis (5.2.3).

5.4 Double RNA *trans*-splicing studies in RDEB patient keratinocytes

5.4.1 Cloning of dRTM 31/1-FLAG in a retroviral vector

For endogenous studies dRTM 31/1-FLAG was cloned into the retroviral vector pMX-*IRES*-Blasticidin (Clontech, Mountain View, CA, USA) to facilitate the detection of restored *COL7A1* in RDEB patient cell lines. To enhance the expression of the dRTM a CMV promotor was additionally inserted.

First, the CMV promotor was PCR amplified using the GoTaq DNA polymerase (Promega, Madison, MI, USA) and the pcDNA 4.0 vector as template, a CMV specific forward primer (5'-GATCGGATCCGACATTGATTATTGACTAGTTATTAATAGTAATCAATTACG-3') containing a BamHI restriction site and a CMV specific reverse primer with an EcoRI restriction site binding behind the tet-operator of the pcDNA 4.0 vector (5'-GATCGAATTCCGGAGGCTGGATCGGTCCCGGT-3'). Figure 28 shows the vector map of pcDNA 4.0.

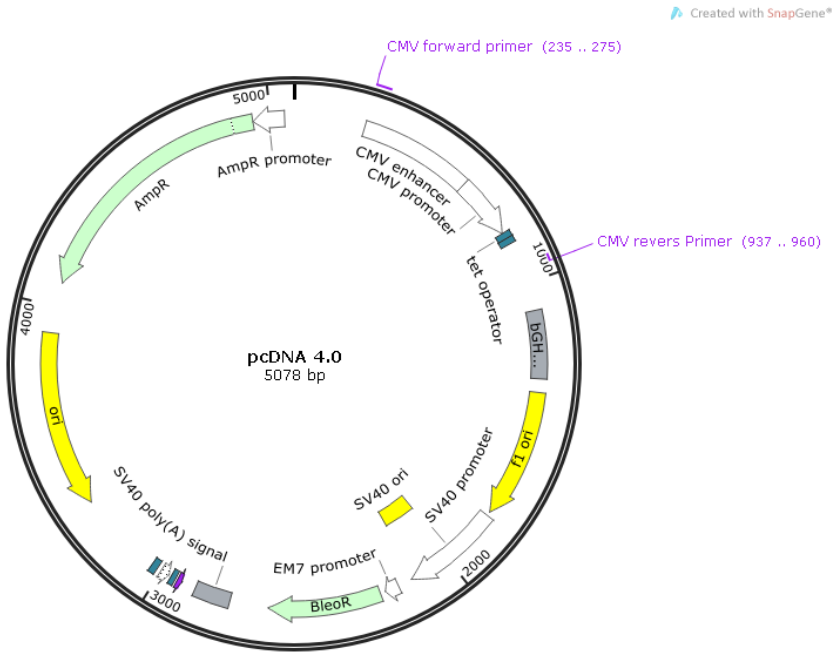

Figure 28. Vector map of pcDNA 4.0. The binding positions of the primers for PCR amplification of CMV are marked in purple. Plasmid map was generated using SnapGene® Viewer 2.3.3.

The CMV promotor was cloned into the pMX-*IRES*-Blasticidin vector by BamHI and EcoRI (FastDigest Enzymes of Thermo Fisher Scientific, Waltham, MA, USA) according to the manufacturer's protocol. The right orientation and position of CMV within the retroviral vector was confirmed by sequence analysis (5.2.3).

Afterwards 2 µg of pcDNA vector harbouring dRTM 31/1-FLAG and 2 µg of pMX-*IRES*-Blasticidin_CMV were digested with the restriction enzyme EcoRI. dRTM 31/1-FLAG was subsequently cloned into the pMX-*IRES*-Blast_CMV vector. The proper cloning of the dRTM 31/1-FLAG into the retroviral vector containing the CMV promoter was verified by sequence analysis. Figure 29 shows the newly created plasmid pMX-*IRES*-Blasticidin_CMV dRTM 31/1-FLAG.

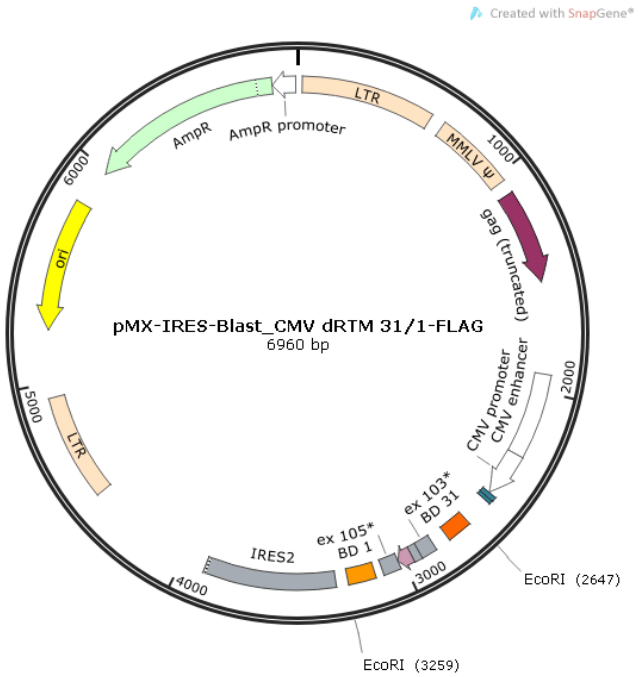

Figure 29. pMX-*IRES*-Blasticidin containing CMV promotor and dRTM 31/1-FLAG. The binding domains BD 31 and BD 1 of dRTM 31/1-FLAG are marked in light and dark orange. 3x FLAG tag is visualised as a pink arrow. CMV is shown in white and *IRES 2* in grey. Plasmid map was generated using SnapGene® Viewer 2.3.3.

5.4.2 Transient transfection of RDEB keratinocytes

For endogenous studies 2,5 µg of dRTM 31/1-FLAG in pMX-*IRES*-Blast_CMV were transfected into immortalized RDEB patient keratinocytes (mutation in exon 80 6527insC) using Xfect™ Transfection Reagent (Clontech Laboratories, Inc. A Takara Bio Company). Transfections were done as proposed by Clontech Laboratories Protocol.

5.4.3 Nested RT-PCR for detection of accurate double *trans*-splicing

For detection of *trans*-splicing induced by dRTM 31/1-FLAG nested RT-PCR on total RNA of transfected RDEB cells were performed using GoTaq DNA polymerase (Promega, Madison, MI, USA). The first PCR was done using *COL7A1* exon 102 specific forward primer (5'-GTGACAAAGGACCTCGGGGAGAC-3') and exon 106 binding reverse primer (5'-CAAGGCCACAGGCTCCCTTCAC-3'). The PCR was done by standard protocol conditions with an annealing temperature of 60°C, an extension time of 20 seconds and 50 cycles. The *trans*-splicing product above the *cis*-splicing product was excised from an agarose gel and used as template for further nested *trans*-splicing PCRs. To prove 3' *trans*-splicing the forward primer applied in the first PCR and a 3x FLAG tag specific reverse primer (5'-CTTGTCATCGTCATCCTT-GTAGTCGATG-3') were used. 5' *trans*-splicing was detected by a 3x FLAG tag binding forward primer (5'-CCATGACGGTGATTATAAAGATCATGACATCG-3') and the reverse primer used in the first PCR. The annealing temperature used for nested PCR was 61°C. All RT-PCR products were confirmed by sequence analysis (5.2.3).

5.4.4 Cloning of dRTM 31/1 in a lentiviral vector

To stably integrate the double RNA *trans*-splicing molecule in RDEB patient keratinocytes and to get a higher *trans*-splicing efficiency, the dRTM 31/1 was cloned into the lentiviral vector pLJM1-*EGFP.* The pLJM1-EGFP vector was kindly provided by David Sabatini of the Whitehead Institute for Biomedical Research in Cambridge (UK). pMX-*IRES*-Blast_CMV carrying dRTM 31/1 was applied as template to PCR amplify dRTM 31/1-*IRES* by using BD 31 forward primer containing an AgeI restriction site (5'-GATCG CTAGCGCCCCTTCATGGGGCCAATC-3') and *IRES* reverse primer comprising a NheI restriction site (5'-GATCACCGGTGGTTGTGGCCATATTATCAT-3'). The PCR amplified dRTM 31/1-*IRES* was cloned into the pLJM1-*EGFP* vector using AgeI and NheI (FastDigest Enzymes of Thermo Fisher Scientific, Waltham, MA, USA). The cloning of dRTM 31/1-*IRES* into pLJM1-*EGFP* was verified by sequence analysis. The newly generated construct is shown in Figure 30.

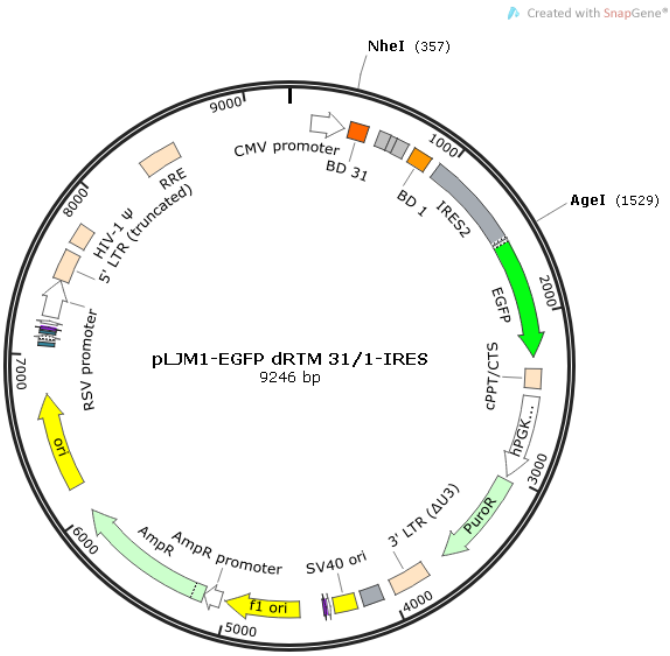

Figure 30. Lentiviral plasmid pLJM1-*EGFP* dRTM 31/1-*IRES*. The binding domains BD 31 and BD 1 are marked in light and dark orange, exon 103 to exon 105 in light grey and *IRES 2* in dark grey. The reporter *EGFP* is shown in green. Plasmid map was generated using SnapGene® Viewer 2.3.3.

5.4.5 Lentiviral transduction of RDEB patient keratinocytes

For a stable integration of the *trans*-splicing molecule dRTM 31/1 in RDEB patient keratinocytes, these cells were transduced via a lentiviral vector system. HEK293 FT cell line (Invitrogen, Carlsbad, CA; [78]) was used for the production of lentiviral particles. For the proper packaging of the lentivirus a 2nd generation lentiviral system was established. The protocol for lentiviral production and transduction was slightly modified from the protocol of Kaspar *et al*. (2007) [78]. The vectors for lentiviral production, phCMV8.91 was kindly provided by Prof. Axel Schambach from the MHH Hannover (Germany) and pMD2.G was kindly provided by Didier Trono of the Ecole Polytechnique Federale de Lausanne (EPFL) and Swiss Federal Institute of Technology (EPFL) in Lausanne (Switzerland).

One day prior to transfection $1{,}7*10^6$ HEK293 FT cells were plated in 10 cm dishes in Hyclone DMEM (GE Healthcare, Little Chalfont, UK) supplemented with 10 % FCII, L-Glu and Na-Pyruvat. Next day at a confluency of 70-95 %, HEK293 FT cells were transfected using a standard calciumphosphat transfection [78], 2-3 hours prior to transfection culture medium was exchanged. Second generation lentiviral packaging plasmids and transfection mix for calciumphosphat transfection are shown in Table 1.

After transfection 0,5 mg/ml geneticin (G418) (Calbiochem, Merck KGaA, Grafing, GER), were added to Hyclone DMEM (+ 10 % FCII, L-Glu and Na-Pyruvat) and HEK293 FT cells were incubated at 32°C, 5 % CO_2 overnight. On day 3 medium was changed to Hyclone DMEM medium (GE Healthcare, Little Chalfont, UK) plus 10 % FCII containing 0,5 mg/ml geneticin for virus production and incubated overnight at 32°C. On day 4 and 5 virus supernatant was harvested, collected, filtered through a 0,45 µm filter to remove cell debris and stored at 4°C. RDEB patient keratinocytes should be at a confluency of 50-60 % prior to transduction. To enhance the transduction efficiency 8 µg/ml polybrene (Sigma-Aldrich, St. Louis, MO, USA) were added to the RDEB cell line together with the viral particles and were centrifuged at 600 g for 1 h at 37°C. Afterwards the cells were cultivated for two hours at 32°C and then at 37°C humid atmosphere overnight. Virus was removed next day, cells were washed four times in PBS and cultivated for 48 hours under normal conditions in SFM medium. Approximately 72 hours after transduction, selection using 1 µl/ml puromycin (InvivoGen, San Diego, CA, USA) was started, because pLJM1-*EGFP* is carrying a puromycin selection cassette. Additionally one flask with not transduced RDEB keratinocytes served as selection control.

Table 1. Applied plasmids and reagents for the production of lentiviral particles.

2nd generation lentiviral packaging	**Plasmids**
Lentiviral transfer vector	pLJM1-*EGFP* dRTM 31/1
Packaging plasmid	phCMV8.91
Envelope plasmid	pMD2.G

Lentiviral transfection mixture	**Components**
Solution A	20 µg pLJM1-*EGFP*
	15 µg phCMV8.91
	5 µg pMD2.G
	80 µl 2,5 M $CaCl_2$
	add H2O to 800 µl
Solution B	800 µl 2x HBS

This transduction by means of 2nd generation lentiviral system led to RDEB patient keratinocytes, where dRTM 31/1 was stable integrated into the genome.

5.4.6 Isolation of genomic DNA and integration PCR

To check for example the integration of dRTM 31/1 in the genome of RDEB keratinocytes, cells were harvested and genomic DNA was isolated using E.Z.N.A.® Blood DNA Mini Kit (Omega Bio-tek, Inc., Norcross, GA, USA) performed by manufacture's protocol. Isolated genomic DNA was stored at -20°C.

The integration of dRTM 31/1 was checked by PCR using a CMV forward primer (5'-TGGATAGCGGTTTGACTCAC-3') and a exon 105 of *COL7A1* reverse primer (5'-TGGATAGCGGTTTGACTCAC-3'), a exon 103 forward primer (5'-CTCCGCCGGGCTGCCTG-3') and an *IRES* reverse primer (5'-GACGGCAATATGGTGGAAAATAAC-3').

5.4.7 Immunofluorescence microscopy

To investigate the rescue of type VII collagen maintained via double RNA *trans*-splicing, immunofluorescence staining was performed. Applying this method makes it possible to observe a specific protein expression and its localisation in the cell based on the interaction of a specific antibody and the antigen illustrated by a fluorescent dye labelled secondary antibody [79]. For this specific characterization of the protein 80.000 cells (humane keratinocytes, RDEB cell line, transduced RDEB cell line) were seeded in chamber slides (Sigma Aldrich, St. Louis, MO, USA) and grown in supplemented SFM Medium until they reached a confluency of 70 - 80 %. Cells were washed in PBS and fixed using 4 % formaldehyde (Sigma Aldrich, St. Louis, MO, USA) by incubation at room temperature for 30 minutes. To remove all of the formaldehyde the cells were washed 3 times in PBS. To block unspecific binding sites, the cells were treated with 1 % Bovine Serum Albumin (Sigma Aldrich, St. Louis, MO, USA) and 0,5 % Triton X-100 (Sigma Aldrich, St. Louis, MO, USA) in PBS for 45 minutes. Cells were washed again and incubated with the primary polyclonal antibody anti type VII collagen LH7.2 produced in rabbit (1:3000 diluted in PBS) for two hours at room temperature. Thereafter cells were washed three times in PBS again and got incubated with the secondary antibody Alexa Fluor 594 goat anti-rabbit IgG (H+L) (Life Technologies, Carlsbad, CA, USA ; 1:400 dilution in PBS) for another hour in the dark. Then there were washing steps (three times in PBS) and the nuclei of the

cells were stained by 4',6-diamidino-2-phenylindole (DAPI) (Sigma-Aldrich, St. Louis, MO, USA) in 1:3000 dilution for 10 minutes. After the last washing step, the cells were embedded in mounting medium (Dako, Agilent Technologies, Santa Carla, CA, USA). The collagen type VII staining was visualized via fluorescence microscopy (Axiophot, Carl Zeiss, Oberkochen, GER).

6 References

1. Institute for Quality and Efficiency in Health Care. How does the skin work? *PubMed Health* **2016**.
2. Kanitakis, J. Anatomy, histology and immunohistochemistry of normal human skin. *European Journal of Dermatology* **2002**, *12*, 390–401.
3. MacNeil, S. Progress and opportunities for tissue-engineered skin. *Nature* **2007**, *445*, 874–880.
4. Speckmann, E.J.; Hescheler, J.; Köhling, R. *Physiologie*, 5th ed; Elsevier Urban & Fischer: München, 2009.
5. Proksch, E.; Brandner, J.M.; Jensen, J.-M. The skin: An indispensable barrier. *Experimental Dermatology* **2008**, *17*, 1063–1072.
6. Kolarsick, P.A.J.; Kolarsick, M.A.; Goodwin, C. Anatomy and Physiology of the Skin. *Journal of the Dermatology Nurses' Association* **2011**, *3*, 203–213.
7. Breitkreutz, D.; Mirancea, N.; Nischt, R. Basement membranes in skin: Unique matrix structures with diverse functions? *Histochem Cell Biol* **2009**, *132*, 1–10.
8. Fine, J.-D. Inherited epidermolysis bullosa. *Orphanet J Rare Dis* **2010**, *5*, 12.
9. Boeira, V.; Rocha, B.; et al. Inherited epidermolysis bullosa: clinical and therapeutic aspects. *Anais Brasileiros de Dermatologia* **2013**, *88*, 185–198.
10. DEBRA Austria. *Epidermolysis bullosa - Erkrankung*. Available online: http://www.debra-austria.org/startseite.html (accessed on 29 April, 2016).
11. McGrath, J.A. Recently Identified Forms of Epidermolysis Bullosa. *Ann Dermatol* **2015**, *27*, 658.
12. Fine, J.-D.; Bruckner-Tuderman, L.; Eady, R.A.; Bauer, E.A.; Bauer, J.W.; Has, C.; Heagerty, A.; Hintner, H.; Hovnanian, A.; Jonkman, M.F.*; et al.* Inherited epidermolysis bullosa: Updated recommendations on diagnosis and classification. *Journal of the American Academy of Dermatology* **2014**, *70*, 1103–1126.
13. Werner, N.S.; Windoffer, R.; Strnad, P. Epidermolysis Bullosa Simplex-Type Mutations Alter the Dynamics of the Keratin Cytoskeleton and Reveal a Contribution of Actin to the Transport of Keratin Subunits. *Molecular Biology of the Cell* **2004**, *15*, 990–1002.
14. Coulombe, P.A.; Kerns, M.L.; Fuchs, E. Epidermolysis bullosa simplex: A paradigm for disorders of tissue fragility. *J. Clin. Invest.* **2009**, *119*, 1784–1793.

15. Kiritsi, D.; Cosgarea, I.; Franzke, C.-W.; Schumann, H.; Oji, V.; Kohlhase, J.; Bruckner-Tuderman, L.; Has, C. Acral Peeling Skin Syndrome with TGM5 Gene Mutations May Resemble Epidermolysis Bullosa Simplex in Young Individuals. *Journal of Investigative Dermatology* **2010**, *130*, 1741–1746.
16. University of Washington, Seattle. *Junctional Epidermolysis Bullosa*; 2014. Available online: http://www.ncbi.nlm.nih.gov/books/NBK1125/?report=reader#ebj.Molecular_Genetics (accessed on 29 April, 2016).
17. Ashton, G. Kindler syndrome. *Clinical and Experimental Dermatology* **2004**, *29*, 116–121.
18. Dang, N.; Murrell, D.F. Mutation analysis and characterization of COL7A1 mutations in dystrophic epidermolysis bullosa. *Exp Dermatol* **2008**, *17*, 553–568.
19. Chung, H.J.; Uitto, J. Type VII Collagen: The Anchoring Fibril Protein at Fault in Dystrophic Epidermolysis Bullosa. *Dermatologic Clinics* **2010**, *28*, 93–105.
20. Fine, J.D.; Hintner, H. *Life with Epidermolysis Bullosa (EB)*: *Etiology, Diagnosis, Multidisciplinary Care and Therapy*; Springer-Verlag: Wien, 2009.
21. Soro, L.; Bartus, C.; Purcell, S. Recessive Dystrophic Epidermolysis Bullosa: A Review of Disease Pathogenesis and Update on Future Therapies. *The Journal of Clinical and Aesthetic Dermatology* **2015**, *8*, 41–46.
22. Intong, L.R.; Murrell, D.F. Inherited epidermolysis bullosa: New diagnostic criteria and classification. *Clinics in Dermatology* **2012**, *30*, 70–77.
23. Dédée, F.M. *Blistering Diseases*: *Clinical Features, Pathogenesis, Treatment*; Springer-Verlag: Berlin, 2015.
24. Wagner John E.; Ishida-Yamamoto Akemi; McGrath John A.; Hordinsky Maria; Keene Douglas R.; Woodley David T.; Chen Mei; Riddle Megan J.; Osborn Mark J.; Lund Troy*; et al.* Bone Marrow Transplantation for Recessive Dystrophic Epidermolysis Bullosa. *The NEW ENGLAND JOURNAL of MEDICINE* **2010**, *7*, 629–639.
25. Woodley, D.T.; Keene, D.R.; Atha, T.; Huang, Y.; Lipman, K.; Li, W.; Chen, M. Injection of recombinant human type VII collagen restores collagen function in dystrophic epidermolysis bullosa. *Nature medicine* **2004**, *10*, 693–695.
26. Remington, J.; Wang, X.; Hou, Y.; Zhou, H.; Burnett, J.; Muirhead, T.; Uitto, J.; Keene, D.R.; Woodley, D.T.; Chen, M. Injection of recombinant human type VII collagen corrects the disease phenotype in a murine model of dystrophic epidermolysis bullosa. *Molecular therapy : the journal of the American Society of Gene Therapy* **2009**, *17*, 26–33.

27. Baldeschi, C.; Gache, Y.; Rattenholl, A.; Bouille, P.; Danos, O.; Ortonne, J.-P.; Bruckner-Tuderman, L.; Meneguzzi, G. Genetic correction of canine dystrophic epidermolysis bullosa mediated by retroviral vectors. *Human Molecular Genetics* **2003**, *12*, 1897–1905.
28. Sat, E.; Leung, K.H.; Bruckner-Tuderman, L.; Cheah, K.S. Tissue-specific expression and long-term deposition of human collagen VII in the skin of transgenic mice: implications for gene therapy. *Gene therapy* **2000**, *7*, 1631–1639.
29. Woodley, D.T.; Keene, D.R.; Atha, T.; Huang, Y.; Ram, R.; Kasahara, N.; Chen, M. Intradermal injection of lentiviral vectors corrects regenerated human dystrophic epidermolysis bullosa skin tissue in vivo. *Molecular therapy : the journal of the American Society of Gene Therapy* **2004**, *10*, 318–326.
30. Ortiz-Urda, S.; Thyagarajan, B.; Keene, D.R.; Lin, Q.; Fang, M.; Calos, M.P.; Khavari, P.A. Stable nonviral genetic correction of inherited human skin disease. *Nature medicine* **2002**, *8*, 1166–1170.
31. Gache, Y.; Baldeschi, C.; Del Rio, M.; Gagnoux-Palacios, L.; Larcher, F.; Lacour, J.-P.; Meneguzzi, G. Construction of skin equivalents for gene therapy of recessive dystrophic epidermolysis bullosa. *Human gene therapy* **2004**, *15*, 921–933.
32. Titeux, M.; Pendaries, V.; Zanta-Boussif, M.A.; Decha, A.; Pironon, N.; Tonasso, L.; Mejia, J.E.; Brice, A.; Danos, O.; Hovnanian, A. SIN retroviral vectors expressing COL7A1 under human promoters for ex vivo gene therapy of recessive dystrophic epidermolysis bullosa. *Molecular therapy : the journal of the American Society of Gene Therapy* **2010**, *18*, 1509–1518.
33. Siprashvili, Z.; Nguyen, N.T.; Bezchinsky, M.Y.; Marinkovich, M.P.; Lane, A.T.; Khavari, P.A. Long-term type VII collagen restoration to human epidermolysis bullosa skin tissue. *Human gene therapy* **2010**, *21*, 1299–1310.
34. Goto, M.; Sawamura, D.; Ito, K.; Abe, M.; Nishie, W.; Sakai, K.; Shibaki, A.; Akiyama, M.; Shimizu, H. Fibroblasts show more potential as target cells than keratinocytes in COL7A1 gene therapy of dystrophic epidermolysis bullosa. *The Journal of investigative dermatology* **2006**, *126*, 766–772.
35. Woodley, D.T.; Krueger, G.G.; Jorgensen, C.M.; Fairley, J.A.; Atha, T.; Huang, Y.; Chan, L.; Keene, D.R.; Chen, M. Normal and gene-corrected dystrophic epidermolysis bullosa fibroblasts alone can produce type VII collagen at the basement membrane zone. *The Journal of investigative dermatology* **2003**, *121*, 1021–1028.

36. Wong, T.; Gammon, L.; Liu, L.; Mellerio, J.E.; Dopping-Hepenstal, P.J.C.; Pacy, J.; Elia, G.; Jeffery, R.; Leigh, I.M.; Navsaria, H.*; et al.* Potential of fibroblast cell therapy for recessive dystrophic epidermolysis bullosa. *The Journal of investigative dermatology* **2008**, *128*, 2179–2189.
37. Fritsch, A.; Loeckermann, S.; Kern, J.S.; Braun, A.; Bosl, M.R.; Bley, T.A.; Schumann, H.; Elverfeldt, D. von; Paul, D.; Erlacher, M.*; et al.* A hypomorphic mouse model of dystrophic epidermolysis bullosa reveals mechanisms of disease and response to fibroblast therapy. *The Journal of clinical investigation* **2008**, *118*, 1669–1679.
38. Petrof, G.; Martinez-Queipo, M.; Mellerio, J.E.; Kemp, P.; McGrath, J.A. Fibroblast cell therapy enhances initial healing in recessive dystrophic epidermolysis bullosa wounds: results of a randomized, vehicle-controlled trial. *The British journal of dermatology* **2013**, *169*, 1025–1033.
39. Tolar, J.; McGrath, J.A.; Xia, L.; Riddle, M.J.; Lees, C.J.; Eide, C.; Keene, D.R.; Liu, L.; Osborn, M.J.; Lund, T.C.*; et al.* Patient-specific naturally gene-reverted induced pluripotent stem cells in recessive dystrophic epidermolysis bullosa. *The Journal of investigative dermatology* **2014**, *134*, 1246–1254.
40. Chamorro, C.; Mencia, A.; Almarza, D.; Duarte, B.; Buning, H.; Sallach, J.; Hausser, I.; Del Rio, M.; Larcher, F.; Murillas, R. Gene Editing for the Efficient Correction of a Recurrent COL7A1 Mutation in Recessive Dystrophic Epidermolysis Bullosa Keratinocytes. *Molecular therapy. Nucleic acids* **2016**, *5*, e307.
41. Osborn, M.J.; Starker, C.G.; McElroy, A.N.; Webber, B.R.; Riddle, M.J.; Xia, L.; DeFeo, A.P.; Gabriel, R.; Schmidt, M.; Kalle, C. von*; et al.* TALEN-based gene correction for epidermolysis bullosa. *Molecular therapy : the journal of the American Society of Gene Therapy* **2013**, *21*, 1151–1159.
42. Sebastiano, V.; Zhen, H.H.; Haddad, B.; Bashkirova, E.; Melo, S.P.; Wang, P.; Leung, T.L.; Siprashvili, Z.; Tichy, A.; Li, J.*; et al.* Human COL7A1-corrected induced pluripotent stem cells for the treatment of recessive dystrophic epidermolysis bullosa. *Science translational medicine* **2014**, *6*, 264ra163.
43. Murauer, E.M.; Gache, Y.; Gratz, I.K.; Klausegger, A.; Muss, W.; Gruber, C.; Meneguzzi, G.; Hintner, H.; Bauer, J.W. Functional Correction of Type VII Collagen Expression in Dystrophic Epidermolysis Bullosa. *Journal of Investigative Dermatology* **2011**, *131*, 74–83.

44. Featherstone, C. Epidermolysis bullosa: from fundamental molecular biology to clinical therapies. *The Journal of investigative dermatology* **2007**, *127*, 256–259.
45. Peking, P.; Koller, U.; Hainzl, S.; Kitzmueller, S.; Kocher, T.; Mayr, E.; Nyström, A.; Lener, T.; Reichelt, J.; Bauer, J.W.*; et al.* A Gene Gun-mediated Nonviral RNA trans-splicing Strategy for Col7a1 Repair. *Molecular therapy. Nucleic acids* **2016**, *5*, e287.
46. Sullenger, B.A. Targeted genetic repair: An emerging approach to genetic therapy. *J. Clin. Invest.* **2003**, *112*, 310–311.
47. Yang, Y.; Walsh, C.E. Spliceosome-mediated RNA trans-splicing. *Molecular therapy: the journal of the American Society of Gene Therapy* **2005**, *12*, 1006–1012.
48. Faustino, N.A.; Cooper, T.A. Pre-mRNA splicing and human disease. *Genes & Development* **2003**, *17*, 419–437.
49. Garcia-Blanco, M.A.; Baraniak, A.P.; Lasda, E.L. Alternative splicing in disease and therapy. *Nat Biotechnol* **2004**, *22*, 535–546.
50. Mansfield, S.G.; Kole, J.; Puttaraju, M.; Yang, C.C.; Garcia-Blanco; MA; Cohn, J.A.; Mitchell, L.G. Repair of CFTR mRNA by spliceosome-mediated RNA trans-splicing. *Gene Ther* **2000**, *7*, 1885–1895.
51. Mansfield, S.G.; Chao, H.; Walsh, C.E. RNA repair using spliceosome-mediated RNA trans-splicing. *Trends in molecular medicine* **2004**, *10*, 263–268.
52. Koller, U.; Wally, V.; Bauer, J.W.; Murauer, E.M. Considerations for a Successful RNA Trans-splicing Repair of Genetic Disorders. *Mol Ther Nucleic Acids* **2014**, *3*, e157.
53. Berger, A.; Maire, S.; Gaillard, M.-C.; Sahel, J.-A.; Hantraye, P.; Bemelmans, A.-P. mRNA trans-splicing in gene therapy for genetic diseases. *Wiley interdisciplinary reviews. RNA* **2016**.
54. Wally, V.; Murauer, E.M.; Bauer, J.W. Spliceosome-Mediated Trans-Splicing: The Therapeutic Cut and Paste. *Journal of Investigative Dermatology* **2012**, *132*, 1959–1966.
55. Philippi, S.; Lorain, S.; Beley, C.; Peccate, C.; Precigout, G.; Spuler, S.; Garcia, L. Dysferlin rescue by spliceosome-mediated pre-mRNA trans-splicing targeting introns harbouring weakly defined 3' splice sites. *Human Molecular Genetics* **2015**, *24*, 4049–4060.
56. Gruber, C.; Gratz, I.K.; Murauer, E.M.; Mayr, E.; Koller, U.; Bruckner-Tuderman, L.; Meneguzzi, G.; Hintner, H.; Bauer, J.W. Spliceosome-Mediated RNA Trans-Splicing Facilitates Targeted Delivery of Suicide Genes to Cancer Cells. *Molecular Cancer Therapeutics* **2011**, *10*, 233–241.

57. Coady, T.H.; Lorson, C.L. Trans-Splicing-Mediated Improvement in a Severe Mouse Model of Spinal Muscular Atrophy. *Journal of Neuroscience* **2010**, *30*, 126–130.
58. Wang, J.; Mansfield, S.G.; Cote, C.A.; Du Jiang, P.; Weng, K.; Amar, M.J.A.; Brewer, B.H., JR; Remaley, A.T.; McGarrity, G.J.; Garcia-Blanco, M.A.*; et al.* Trans-splicing into highly abundant albumin transcripts for production of therapeutic proteins in vivo. *Molecular therapy : the journal of the American Society of Gene Therapy* **2009**, *17*, 343–351.
59. Chen, H.; Kathirvel, P.; Yee, W.; PS Lai, P. Correction of dystrophia myotonica type 1 pre-mRNAtranscripts by artificial trans-splicing. *Gene therapy* **2009**, *16*, 211–217.
60. Mearini, G.; Stimpel, D.; Kramer, E.; Geertz, B.; Braren, I.; Gedicke-Hornung, C.; Precigout, G.; Muller, O.J.; Katus, H.A.; Eschenhagen, T.*; et al.* Repair of Mybpc3 mRNA by 5'-trans-splicing in a Mouse Model of Hypertrophic Cardiomyopathy. *Molecular therapy. Nucleic acids* **2013**, *2*, e102.
61. Wally, V.; Brunner, M.; Lettner, T.; Wagner, M.; Koller, U.; Trost, A.; Murauer, E.M.; Hainzl, S.; Hintner, H.; Bauer, J.W. K14 mRNA reprogramming for dominant epidermolysis bullosa simplex. *Human Molecular Genetics* **2010**, *19*, 4715–4725.
62. Kierlin-Duncan, M.N.; Sullenger, B.A. Using 5'-PTMs to repair mutant beta-globin transcripts. *RNA (New York, N.Y.)* **2007**, *13*, 1317–1327.
63. Mansfield, S.; Hawkins Clark, R.; Puttaraju, M.; Kole, J. 5' Exon replacement and repair by spliceosome-mediated RNA trans-splicing. *RNA* **2003**, *9*, 1290–1297.
64. Lorain, S.; Peccate, C.; Le Hir, M.; Garcia, L.; Lewin, A. Exon Exchange Approach to Repair Duchenne Dystrophin Transcripts. *PLoS ONE* **2010**, *5*, e10894.
65. Puttaraju, M. Messenger RNA Repair and Restoration of Protein Function by Spliceosome-Mediated RNA Trans-Splicing. *Molecular Therapy* **2001**, *4*, 105–114.
66. Berger, A.; Lorain, S.; Josephine, C.; Desrosiers, M.; Peccate, C.; Voit, T.; Garcia, L.; Sahel, J.-A.; Bemelmans, A.-P. Repair of rhodopsin mRNA by spliceosome-mediated RNA trans-splicing: a new approach for autosomal dominant retinitis pigmentosa. *Molecular therapy : the journal of the American Society of Gene Therapy* **2015**, *23*, 918–930.
67. Koller, U.; Wally, V.; Mitchell, L.G.; Klausegger, A.; Murauer, E.M.; Mayr, E.; Gruber, C.; Hainzl, S.; Hintner, H.; Bauer, J.W. A novel screening system improves genetic correction by internal exon replacement. *Nucleic Acids Research* **2011**, *39*, e108.

68. Wally, V.; Koller, U.; W., J. High-Throughput Screening for Highly Functional RNA-Trans-Splicing Molecules: Correction of Plectin in Epidermolysis Bullosa Simplex. In *Human Genetic Diseases - Dr. Dijana Plaseska-Karanfilska InTech 2011*, pp. 223–240.
69. Bauer, J.W.; Murauer, E.M.; Wally, V.; Koller, U. RNA Trans-Splicing for Genodermatoses. In *Molecular dermatology*: *Methods and protocols*; Has, C., Sitaru, C., Eds.: Humana Press: New York, 2013; Volume 961, pp. 441–455.
70. Koller, U.; Hainzl, S.; Kocher, T.; Hüttner, C.; Klausegger, A.; Gruber, C.; Mayr, E.; Wally, V.; Bauer, J.; Murauer, E. Trans-Splicing Improvement by the Combined Application of Antisense Strategies. *IJMS* **2015**, *16*, 1179–1191.
71. Hua, Y.; Vickers, T.A.; Okunola, H.L.; Bennett, C.F.; Krainer, A.R. Antisense Masking of an hnRNP A1/A2 Intronic Splicing Silencer Corrects SMN2 Splicing in Transgenic Mice. *The American Journal of Human Genetics* **2008**, *82*, 834–848.
72. Coady, T.H.; Baughan, T.D.; Shababi, M.; Passini, M.A.; Lorson, C.L.; Valcarcel, J. Development of a Single Vector System that Enhances Trans-Splicing of SMN2 Transcripts. *PLoS ONE* **2008**, *3*, e3468.
73. Hüttner, C.; Murauer, E.M.; Hainzl, S.; Kocher, T.; Neumayer, A.; Reichelt, J.; Bauer, J.W.; Koller, U. *Designing efficient double RNA trans-splicing molecules for targeted RNA repair*: Salzburg, 2016.
74. Murauer, E.M.; Koller, U.; Hainzl, S.; Wally, V.; Bauer, J.W. A Reporter-Based Screen to Identify Potent 3' Trans -Splicing Molecules for Endogenous RNA Repair. *Human Gene Therapy Methods* **2013**, *24*, 19–27.
75. Gruber, C.; Koller, U.; Murauer, E.M.; Hainzl, S.; Hüttner, C.; Kocher, T.; South, A.P.; Hintner, H.; Bauer, J.W. The design and optimization of RNA trans-splicing molecules for skin cancer therapy. *Molecular Oncology* **2013**, *7*, 1056–1068.
76. Coady, T.H.; Shababi, M.; Tullis, G.E.; Lorson, C.L. Restoration of SMN function: delivery of a trans-splicing RNA re-directs SMN2 pre-mRNA splicing. *Molecular Therapy* **2007**, *15*, 1471–1478.
77. Lorain, S.; Peccate, C.; Le Hir, M.; Griffith, G.; Philippi, S.; Précigout, G.; Mamchaoui, K.; Jollet, A.; Voit, T.; Garcia, L. Dystrophin rescue by trans-splicing: a strategy for DMD genotypes not eligible for exon skipping approaches. *Nucleic Acids Research* **2013**, *41*, 8391–8402.

78. Kaspar, M.; Regl, G.; Eichberger, T.; Frischauf Anna-Maria; Aberger, F. Efficient Manipulation of Hedgehog/GLI Signaling Using Retroviral Expression Systems. *Methods In molecular Biology™* **2007**, *397*, 67–78.
79. Beutner E.H. Immunofluorescent Staining: The Fluorescent Antibody Method. *Bacteriological Reviews* **1961**, *25*, 49–76.

7 Figures

8 Appendix

8.1 Solutions

50x TAE buffer

2M	Tris (AppliChem GmbH, Darmstadt, GER)
695 mM	NaOAc (Serva Electrophoresis GmbH, Heidelberg, GER)
50 mM	EDTA (Sigma-Aldrich, St. Louis, MO, USA)

Cell culture

Solution A

30 mM	HEPES (Sigma Aldrich, St. Louis, MO, USA)
9 mM	Glucose (Merck KGaA, Grafing, GER)
3 mM	KCl (Merck KGaA, Grafing, GER)
132 mM	NaCl (Merck KGaA, Grafing, GER)
1 mM	$Na_2HPO_4x7H_2O$ (Merck KGaA, Grafing, GER)
0,3 mM	Phenol red (Sigma Aldrich, St. Louis, MO, USA)

10x Trypsin/EDTA

0,5 %	Trypsin (Biochrom, Berlin, GER)
0,2 %	EDTA (Biochrom, Berlin, GER)

in PBS

1x Trypsin/EDTA

1:10 dilution of 10x Trypsin/EDTA in solution A

1x FCS/EDTA

1:10 dilution of FCS (Biochrom, Berlin, GER) in solution A

Freeze Medium

FCS (Biochrom, Berlin, GER) adding 10 % DMSO (Sigma-Aldrich, St. Louis, MO, USA)

LB medium

25 g	Luria Broth (Sigma Aldrich, St. Louis, MO, USA)
1 L	ddH_2O